CRITICAL REVIEW ON EFFECTS OF PORE TYPE CLASSIFICATIONS ON PORE PRESSURE AND ITS ESTIMATION TECHNIQUES

by

Full Name: Muhammad Iqmarul Alimin Bin Md. Sambri
Student ID: G02371

This dissertation report is submitted in partial fulfilment of the requirement for Masters of Science in Petroleum Engineering (MSc PE) Session 2013-2014.

MAY 2014

Universiti Teknologi PETRONAS
Bandar Seri Iskandar 31750
Tronoh, Perak Darul Ridzuan
Malaysia

Certification of Approval

CRITICAL REVIEW ON EFFECTS OF PORE TYPE CLASSIFICATIONS ON PORE PRESSURE AND ITS ESTIMATION TECHNIQUES

by

Full Name: Muhammad Iqmarul Alimin Bin Md. Sambri
Student ID: G02371

A project dissertation submitted to the Petroleum Engineering Programme Universiti Teknologi PETRONAS in partial fulfilment of the requirement for the MSc of PETROLEUM ENGINEERING

Approved by,

_____

Dr Masoud Rashidi
Project Supervisor and Senior Lecturer
Programme Modulator MSc Petroleum Engineering
Universiti Teknologi PETRONAS
Bandar Seri Iskandar 31750
Tronoh, Perak Darul Ridzuan
Malaysia

Certification of Originality

This is to certify that I am responsible for the work submitted in this project, that the original work is my own except as specified in the references and acknowledgements, and that the original work contained herein have not been undertaken or done by unspecified sources or persons.

_____

Muhammad Iqmarul Alimin Bin Md. Sambri G02371

ABSTRACT

Determining pore pressure is one of the main vital factors to be considered in a pre-drilling phase of each development plan. This is because with the right pore pressure estimated, proper casing design and drilling fluid can be used which in turn can save money, lives and environments. If wrongly predicted, accidents and unwanted problems such as blowouts and wellbore instability can occur. In this project study, a relationship between pore types, their classifications with pore pressure was first examined by reviewing previous published works. An indirect correlation was found between pore type and pore pressure but a rather direct correlation for pore type to porosity was found where different pore types and their classifications give different porosity. It was found that there are three different basic types of pores which are reference, stiff and cracks. They are different in aspect ratio corresponding to different porosity values. Hence for a certain porosity value, there must be a certain pore pressure. This pore pressure can be calculated on different methods. The different approaches on prediction methods were assessed and critical evaluation was made on them to find the advantages, disadvantages, limitations and assumptions on each, focusing into solving the problems and as a part of the objectives of this research. The best prediction method chosen was with the use of acoustic or sonic log with electrical log in determining this pore pressure. It also could be combined with the existing core and log data from a field observed.

ACKNOWLEDGEMENTS

First and foremost, all praise to Allah SWT, for without His help this dissertation would not have been possible. I would like to express my sincere gratitude and to acknowledge a list of individuals below for their contributions throughout this project writing.

1) Dr Masoud Rashidi, Project Supervisor and Senior Lecturer, Programme Modulator in MSc Petroleum Engineering at the Universiti Teknologi PETRONAS – for supervising my project writing, for his assistance, guidance and constructive criticism.
2) Associate Professor Dr Ismail Mohd Saaid, Head of Petroleum Engineering at the Universiti Teknologi PETRONAS – for supervising my academic progress, for his support, advice and cooperation.
3) Engineer Saleem Qadir Tunio, Individual Project Coordinator at the Universiti Teknologi PETRONAS – for the constant updates in datelines, reminders and individual project details given.
4) Lecturers and members during the course of study in MSc Petroleum Engineering from the Heriot-Watt University and from the Universiti Teknologi PETRONAS (both in Faculty of Petroleum Engineering and Faculty of Petroleum Geoscience) – for their encouragement and helps.

I wish to extend my deepest gratitude to the Brunei National Petroleum Company Sendirian Berhad (PetroleumBRUNEI) and its staff, for sponsoring and giving me such golden opportunity to undertake and further my study in Masters of Science in Petroleum Engineering at the Universiti Teknologi PETRONAS, Perak, Malaysia. Heartfelt thanks are extended to my parents, families, Abdul Khalliq Kaflee, Dk Norariza PHM, Noradilahyati Hj Abdullah, Liyana Hj Sulaiman, friends and course mates for the constant support, blessings and love conveyed throughout my study.

TABLE OF CONTENTS

LIST OF FIGURES

LIST OF TABLES

ABBREVIATIONS AND NOMENCLATURE

PSD	:	Pore Size Distribution
3-D	:	Three Dimensional
MWD	:	Measurement While Drilling
LWD	:	Logging While Drilling

Chapter 1 INTRODUCTION

1.1 Background of Project

This research study is to find a relationship between pore type and their classifications with pore pressure, if there is. Pore type here includes pore geometry or a range of pore sizes and diameters. The importance of finding pore pressure of subsurface is such that it helps to predict and model what the well design will look like as to maximize profit and safety while minimizing cost of investment in the exploration, drilling and production operations of oil and gas industry (Fertl and Chilingarian, 1977, Smith, 2000). Mainly in a pre-drilling and during drilling phase, this includes in the design of casing with respect to its setting depth, permitting better casing points selection (Foster, 1966), to program type of drilling fluid used (Smith, 2000), in evaluations of reservoirs and overall to design a successful, efficient and safe drilling activities (Hottmann and Johnson, 1965).

Given a geological setting, to predict pore pressure a set of normal parameters are used. There will not be many problems in the design of well if this is the case. However, this is not the usual case. A lot of parameters have caused the pore pressure to be lower or higher than the normal pore pressure. This is called an abnormal pressure. There are a lot of geological effects or mechanisms generating this abnormal pressure as explained in many published papers by Kulkarni, Meyer and Sixta, 1999, Shaker, 2002, Guiterrez, Braunsdorf and Couzens, 2006, Cao et al., 2006), such as:

- Expansion of fluid volume due to heating
- Under compaction (compaction disequilibrium); loading forces by which pore fluids are restricted from moving as there is a fast burial of rocks having sufficiently low permeability
- Compression in lateral direction
- Reservoir depletion
- Movements of Earth's tectonic plates (lateral stress)
- Movement of fluid due to contrast in the lateral density and buoyancy effect.

In a chronological timeline, different methods of determining pore pressure have been used. A lot of these methods have improved, made better amendments with time. With this a relationship between pore type and their classifications is to be observed with pore pressure. Most well-known methods made full use of the porosity as being the main parameter to determine this pore pressure. This porosity is a function of different parameters like effective stress since porosity is a measure of degree of compaction (Hubbert and Rubey, 1959, Guiterrez, Braunsdorf and Couzens, 2006). This means that value of porosity decreases with depth as effective stress increases. So by monitoring changes in porosity which probably has a relation with pore type and their classifications, maybe it is possible to see the changes in pore pressure (Hubbert and Rubey, 1959).

1.2 Problem Statement

To obtain successful drilling activities, determining the correct pore pressure becomes the main key (Hubbert and Rubey, 1959). An integration of data and observations from different sources can provide better result in predicting pore pressure in line with its geological environment settings (Smith, 2000). With a good estimation of pore pressure, the mud weight can then be properly designed

with respect to the correct use of pore pressure gradient resulting in high penetration rate of mud at low cost (Foster, 1966, Lesage et. al, 1992, Smith, 2000). If wrongly set, blowout or kick or lost circulation fluid and instability problems in wellbore may occur (Guiterrez, Braunsdorf and Couzens, 2006). The distribution of pore pressure is different in different parts of the world depending on parameters that vary differently in that specific area of interest. So predicting pore pressure becomes an ultimate goal.

Before drilling, pore pressure is estimated indirectly by use of offset well log data or by analysis of seismic results. An inspection of different velocities in the seismic data helps to identify different zones of hydrocarbon and non-hydrocarbon. This method however is expensive and not quantitative. Offset wells data means analysing the logs given such that those of resistivity, porosity and density logs – more preferable to be applied in pre-drilling phase. However during drilling, it is estimated by the evaluation of real time information. In a specific environment, familiar known methods have been used like: Eaton method, Bowers method and Miller method to obtain this pore pressure.

There has not been much research conducted to examine the relationship between pore types, their classifications with pore pressure. This study attempts to examine possible correlation between pore types, their classifications with pore pressure.

1.3 Objectives and Scope of Study

The objectives of study for this project are:

- To examine possible relationship between pore types, their classifications with pore pressure.
- To identify different methods of pore pressure prediction and use known best method to predict pore pressure. This focuses into solving the problems by using the data given.
- To make future recommendations in obtaining realistic results within the time constraint given.

Scope of study includes published works in the form of journals, books and certified websites. First a discovery is to be made to see if a relationship exists between pore types, their classifications with pore pressure. Then with the proposed objectives, a method is to be applied making a critical evaluation on the research study making full use of the offset well data given. Then a further study between different approaches of pore pressure estimation is to be done then from this, they are to be compared and contrasted to choose the best method that can be applied in this study. Finally, a modification is made if there is an action needed in giving more accurate results.

Acquiring a deeper knowledge on this study comes off as one of the important factors to be considered in the Oil and Gas industry as much failure can be seen to be increasing nowadays. This research study is important because it can save a lot of money and in fact save lives if the correct estimation is done to prevent unwanted problems as stated above from occurring. It is feasible to do this project within a limited timeline given after doing intensive literature based research on this matter. No hardware is needed other than personal computer as this research study is mostly literature based.

Chapter 2 LITERATURE REVIEW

2.1 Pore Types and their Classifications

It was found out there was a limited amount of works done in classifying the different pore types. This is important in this study by which with limited amount of data given, can the different pore types be more understood? Luanxiao Zhao et al., 2013 paper discussed how pore type is distributed quantitatively from data obtained that of offset well logs and seismic. Their paper also detailed out three different types of pores corresponding to different porosities in the pores then representing the effective stresses connection. This revealed the relationship between pore types and their classifications with porosity then to pore pressure.

They also reported that the variations in pore types and their classifications are due to the difference in historical digenesis which affected and changed the texture and mineralogy of the rocks within. Hence if minerals within rocks and their fluids are known, cross-plots of velocity with porosity are related to the type of pore. It was found that there are three basic pore types which are geophysically termed as stiff, reference and crack pores. Their aspect ratios are 0.7-0.8, 0.12-0.15 and 0.01-0.02 respectively. The summary of results from their research and their images are shown in **Figure 2.1** (Irineu and Roseane, 2012, Luanxiao Zhao et al., 2013):

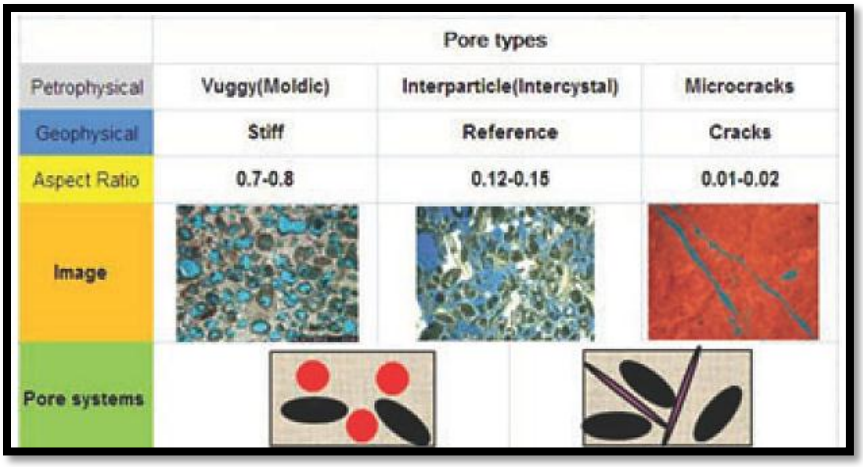

Figure 2.1: Different Pore Types (Luanxiao Zhao et al., 2013)

Geological processes such as dolomitisation, dissolution and cementation in the pores are the main factors affecting porosities. In other words, the spatial distributions of variation in pore types are due to the effect of these processes and their effects towards other petrophysical properties like porosities (Luanxiao et al., 2013). **Figure 2.2** shows for a different pore type and their classifications, how velocity and porosity is related where H-S bounds are Hashin-Shtrikman bounds, reference line is for reference pores as stated in **Figure 2.1**.

Figure 2.2 details out this manner between two stones which are limestone and dolostone. The y-axis represents the velocity while the x-axis represents the porosity values. From their study, it was stated that below the reference line represents more cracks and above reference line represents more stiff pores in the pore type. Velocity is more affected in stiff pores than in crack pores. In a detail manner, shear wave (S-wave velocity) is more affected by cracks than stiff pores (Luanxiao et al., 2013, Irineu and Roseane, 2012).

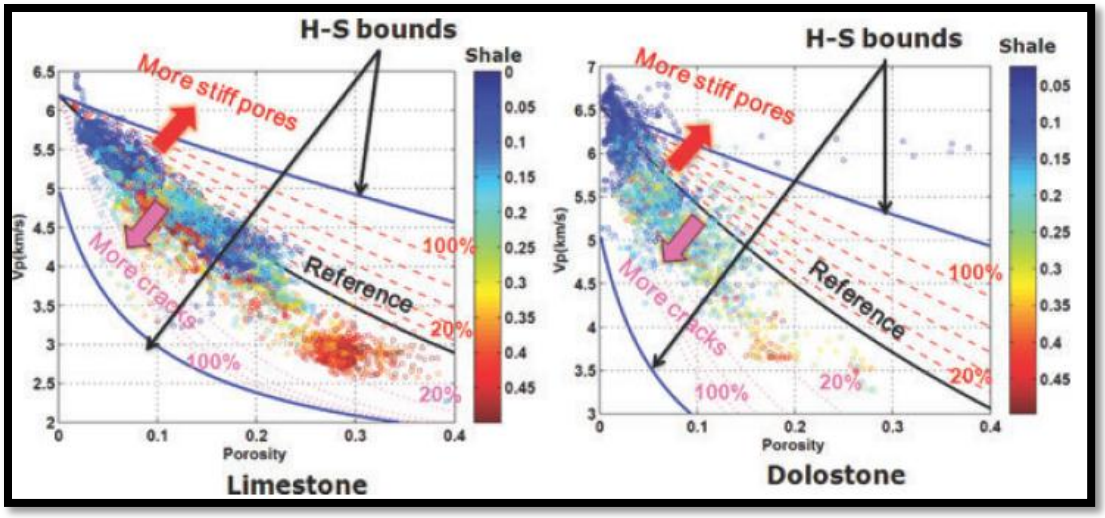

Figure 2.2: Pore Type Effect with Cross-plot of Velocity-Porosity Relation (Luanxiao Zhao et al., 2013)

It is clearly established from critical evaluation of different papers here and the findings from these papers, between pore type and their classifications, there is an indirect relationship between pore type that is pore size and geometry with the pore pressure (Fertl and Chilingarian, 1977), this however need to be comprehended in relation to other properties such that there are different porosities for different pore types and their classifications. For these different porosities, they correspond to different values of pore pressures. Hence there is indeed to understand about this information before proceeding further in comprehending its relationship. With the help of core data, geological data, offset well data and seismic data then their combination can help map the pore size distribution (PSD) in a reservoir.

2.2 Porosity

Porosity is a rock property which characterises pore space (Nimmo, 2004). It is a ratio of void volume to total volume. It depends on particle size distribution, particle shape, cementing and packing density. Depending how the grains are

packed, porosity values, ø must be between 0.26 to 0.48. For sand grains of different sizes, ø is between 0.30 to 0.35 (Nimmo, 2004). If irregularities in shape increase, gaps are getting bigger thus giving bigger porosity. This relates to the PSD.

PSD is usually defined by the effective radius of the pore body. Another factor constituting the effect of size includes cross sectional area and pore volume. PSD is in relative abundance to that of pore size representing the volume overall (Nimmo, 2004). Pore size is measured by means of analysis of individual pore images geometrically, done by using 3-D thin section microscopy imposing impregnation techniques. It can also be predicted from seismic data or physical relationship of rocks or be derived from geostatistical methods (Luanxiao et al., 2013). It plays a key role in quantification of structure. Since different porosities give different PSD and hence different pore types and their classifications, so there is a direct correlation of pore types and their classifications with porosity and therefore porosity with pore pressure is directly related (as different pore types give different pore pressure as stated in the first subsection). Predicting pore pressure based on porosity involves compaction of grains with known compressibility (Swarbrick, 2001) and it has a direct relationship with effective stress. Porosity-effective stress relationship is majorly used in determining pore pressure profiles (Shaker, 2002).

2.3 Effective Stress

Effective stress is the load exerted by matrix rocks' grain-to-grain contacts (Holbrook, 1987) and is acting upward as a force diametrically opposing the overburden pressure (Yoshida, Ikeda and Eaton, 1996). Hubert and Rubey, 1959 stated that an effective stress exerted by porous medium is directly proportional to the degree of compaction. The deeper the depth of burial, the higher the

compaction degree so lower porosity and greater density of shale (SPE, 1983). This effect is further discussed in further sections below in determining normal and abnormal pressures. It is one of the main key factors in determining pore pressure (Alixant and Desbrandes, 1991).

Laws of effective stress was first developed by Terzaghi (Kumar et al., 2010, Atashbari and Tongay, 2012) extended further to comprehend more about this parameter in relation to deformation and permeability was laid out in a paper explained by Warpinski and Teufel, 1992. In their paper, it was stated that effective stress may differ between pore types that of sandstone and chalk due to differential effect in the spherical pores in chalk and slot porosity in that of sandstones. The latter tend to have effective stress approximately closer to unity. Later, it was stated that by numerical simulation, effective stress is a function of geomechanical and geological parameters (Khan, Teufel and Zheng, 2000). Another paper studied this effect for petrophysical rock properties in detail (Shafer, Boitnott and Ewy, 2008).

2.4 Normal and Abnormal Pressure

Direct pressure measurement is fairly impossible in pre-drilling phase (Alixant and Desbrandes, 1991). Difficulties include (Scott and Thomsen, 1993):

1) Difficult in measuring remotely pore pressure, there is always a need in measuring other parameters first. Secondary parameters are sensitive to other factors. From this, assumptions are made with respect to these factors.

2) Measured quantity is poorly resolved and sometimes is very inaccurate due to the involvement of random and systematic errors.

3) Prediction is based on method which is calibrated and smoothed using data from around the borehole and wellbore region which do not represent the pore data overall.

Pore pressure is defined as the difference between overburden and the effective stress (Holbrook and Hauck, 1987). It is measured in sand reservoir and predicted in impermeable layers (Shaker, 2002). Pore pressure refers to fluid pressure in pores which is equivalent to the pressure of hydrostatic when the fluid in pores only supports its overlying weight (Kumar et al., 2010) Normal pressure is defined as formation pressure which is estimated to equal that of fluid hydrostatic pressure of equivalent depth (Hottmann and Johnson, 1965, Fertl and Chilingarian, 1977, Khazanehdari, 2012). Any formation which deviates higher of its pressure than this hydrostatic pressure is called overpressure formation or abnormally pressured.

It is this type of pressure that needs to be considered at much expense for drilling activities to succeed. Factors affecting this abnormal pressure are such as permeability of formation, depositional rate and the ratio of hydrocarbon to non-hydrocarbon (Hubert and Rubey, 1959). A lot of researches have been done to understand this abnormal pressure.

In an environment, a layer of sediments were deposited to sea bottom. With time, more and more layers were deposited on top of one another giving sediments to be compacted together with an increase in an overburden weight (Foster, 1966) Fluid inside pore spaces would be squeezed and in hydraulic communication with fluid in the sediments and above the sea giving pressure noted as hydrostatic pressure (Eaton, 1972, Fertl and Chilingarian, 1977, Khazanehdari, 2012). If this fluid was unable to move from pores when overburden weight increases, the fluid

could not be squeezed resulting in higher fluid pressure than the hydrostatic pressure (Fertl and Chilingarian, 1977, SPE, 1983). This phenomenon resulted in an abnormal pressure (Foster, 1966).

Examples of abnormal pressure depend on the basin history (Yao and Han, 2009) and depositional environments like those sediments deposited in slope or outer shelf environment, in ridges, unconformities and diapiric domes (Martin, 1972, Fertl and Chilingarian, 1977). Hubert and Rubey, 1959 also suggested that abnormal pressure occurred in environments of rapid loading, interbedded sandstones and formations with clays. A worldwide occurrence of abnormal pressure is shown in **Figure 2.3**. This figure established that abnormal pressure may occur at a few 100 feet below surface or to depths at 20,000 feet. There is no doubt; dealing with this abnormal pressure becomes one of the important factors in decision-making in the industry since it greatly affects any Oil and Gas activities especially during drilling phase. With its presence, cost, risk and time increases affecting revenue as shown in **Figure 2.4** where x-axis represents cost, risk and time and y-axis represents well depth. This means in the abnormal pressured regions, there are lots of time, cost and risks involved while it was different and more attainable in a normal pressured region.

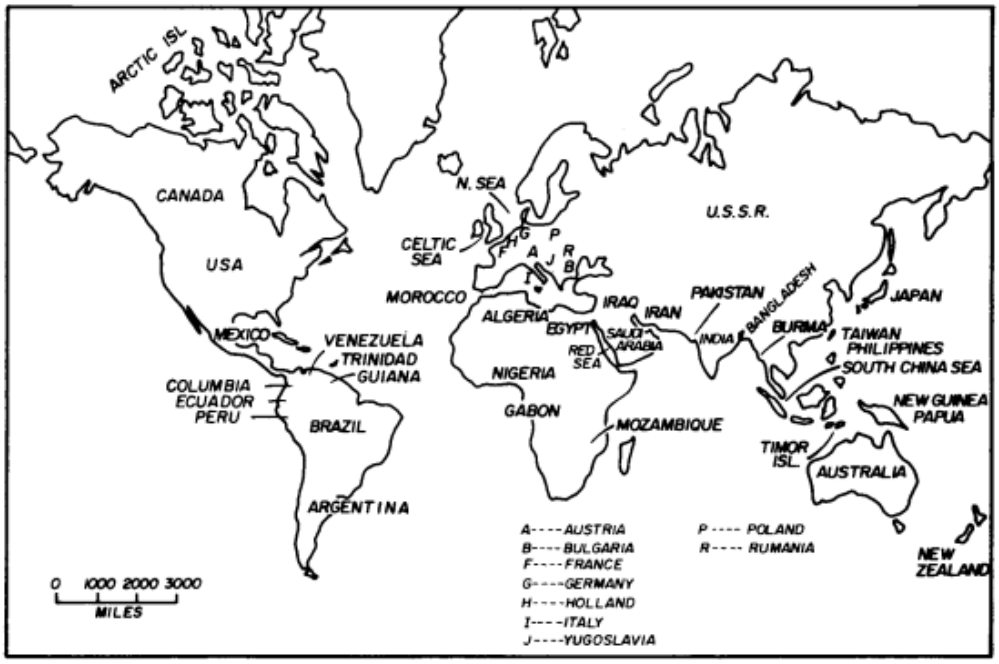

Figure 2.3: The Common Occurrence of Abnormal Pressure Globally (Fertl and Chilingarian, 1977)

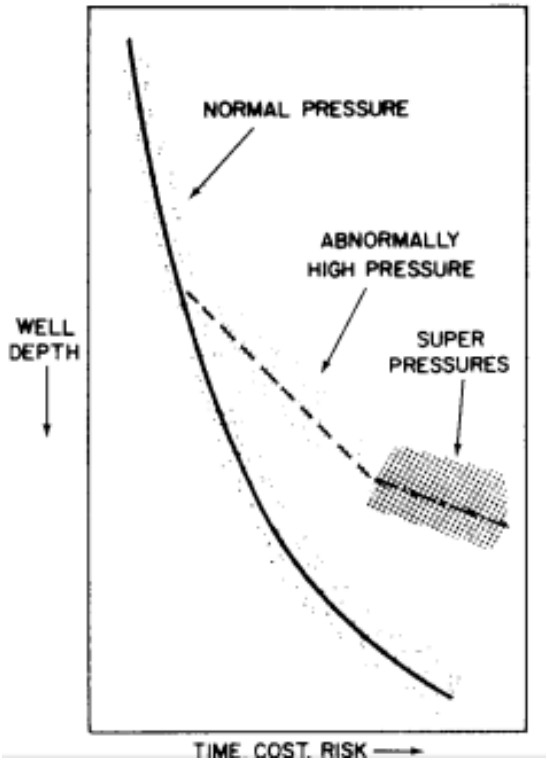

Figure 2.4: Depth vs Time, Cost and Risk for both Normal and Abnormally Pressure Zones (Fertl and Chilingarian, 1977)

2.5 Different Methods of Pore Pressure Estimation

Historically, a deep research has been done for estimating pore pressure using known curves as a function of depth (Holbrook, 1989). The list continues to grow and gets better as time passes by (Bowers, 1995). Scientists and engineers have established curves (Nygaard et al., 2008) which differ in different environmental and formation settings so assumptions have been made throughout with respect to this estimation (Huffman et al., 2011). These prediction methods make full use of seismic data of interval velocities, logs of offset wells and the histories of the wells themselves (Yoshida, Ikeda and Eaton, 1996). Examples of such methods are laid out below, where processes, advantages and limitations of each method are explained briefly.

In estimating this pore pressure, methods are divided into two sections which are argillaceous formations estimation technique and permeable formation estimation technique (Greenword, Dautel and Russell, 2009, Haugland et al., 2013). The first one makes full use of observations corresponding to porosity or effective stress (with comprehension on compaction rate and unloading mechanism which is controlled by size of particles and its distribution, minerals in clay, temperature (Vernik, 2011)) while the second one required direct observation made on pore pressure and knowledge on type of fluid presents and structures geologically. A full case study incorporating all the famous methods was done to a field in Western Canada Sedimentary Basin (Contreras, Hareland and Aguilera, 2011) and also worldwide prediction (Tang et al., 2011), giving different results and noting the differences of good reasons and drawbacks for each method.

2.5.1 Resistivity and Acoustic Logs

Using data from both resistivity and acoustic logs (Hottmann and Johnson, 1965) where a linear relationship between depth and transit time is established while a non-linear relationship is observed between depth and resistivity. C. E Hottmann suggested that both empirical methods (Alixant and Desbrandes, 1991) are accurate at predicting about 0.04 psi/ft fluid pressure gradient while J.F. Evers and Richard of Wyoming in 1983 giving predictions estimated to be accurate at 0.03 psi/ft. This indicates how value is greatly affected by different geological environments and formations as explained in details below.

From the acoustic log, the velocity is a function of lithology and porosity (Hubbert and Rubey, 1959, Khaksar, 2011 and Atashbari and Tingay, 2012) where for a normal trend, a travel time decreases (velocity increases) as porosity decreases since depth increases as shown in **Figure 2.5** where a graph of travel time versus depth is drawn for a normal pressured region. An abnormal trend is observed once deviation occurred from the normal trend due to high transit time since porosity here is higher as shown in **Figure 2.6** where a graph of travel time versus depth is drawn for a normal pressured region as well as an abnormal pressured zone. Note that, velocity is related to density of rock (Rehm and McClendon, 1971). Mathematically, a transit time is related to pore space in rock represented by **Equation 2.1** below where t is transit or travel time, A and B are constants from graph of depth against time and ϕ is porosity (SPE, 1983).

$$\boldsymbol{t = A + B\phi} \qquad \textbf{(2.1)}$$

Detailed description: From these two figures, to estimate pore pressure is first by plotting logarithmic of transit time versus depth then plotting the same graph for

an interested well. If plotted points diverge from the normal line, top of overpressured formation is noted at that specific depth. At any depth, pore pressure can be found by measuring divergence from normal line then find the fluid pressure gradient corresponding to the difference between observe and sand transit times and finally fluid pressure gradient is multiplied to depth to find the pore pressure (Hubbert and Rubey, 1959).

Lane and Macpherson, 1976 reviewed this method in their paper for a case study in the Gulf of Mexico. R. R. Weakley, 1990 also made full use of the sonic or acoustic logs in determining pore pressure for different wells. Miller on the other hand (Zhang, Standifird and Lenamond, 2008), provided, a relationship between effective stress and velocity using normal compaction trend asymptotically to velocities of matrix. All of these papers, established about similar approach.

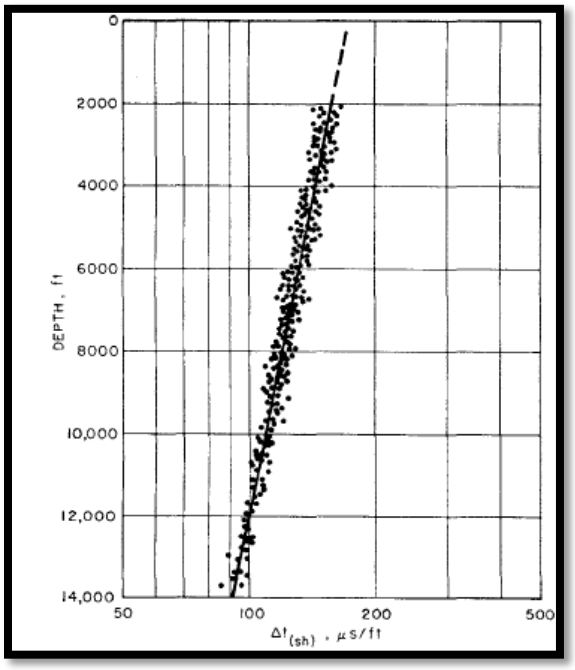

Figure 2.5: Travel Time vs Burial Depth for Normal Pressured (Hottmann and Johnson, 1965)

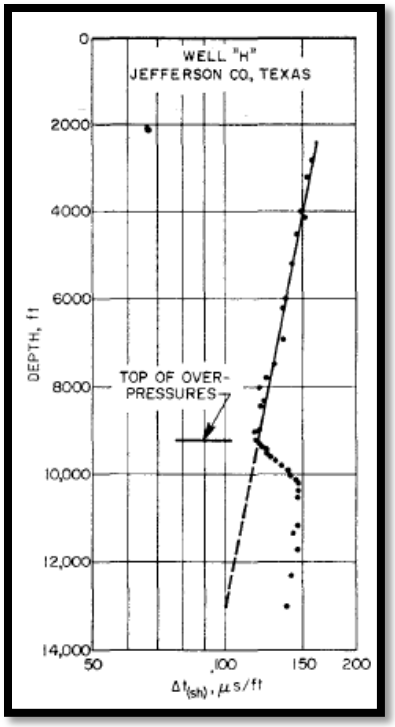

Figure 2.6: Travel Time vs Burial Depth for Abnormal Pressured (Hottmann and Johnson, 1965)

Using resistivity method, factors affecting resistivity are porosity, fluid salinity, mineral composition and temperature (Hubbert and Rubey, 1959, Jones, 1969, SPE, 1983, Haugland and Tichelaar, 2008). Sensitivity of these parameters is explained by Haughland and Tichelaar, 2008. Similarly like the first method, this second method also observed the trend line where resistivity against depth is established as shown in **Figure 2.7**. An abnormal trend is observed one deviation occurred from the normal trend due to lower resistivity observed since porosity is higher (compaction progresses and permeability decreases more rapidly than porosity (Jones, 1969 Eaton, 1975) as shown in **Figure 2.8**. Note that, resistivity and density of rock decreases with burial depth (Martin, 1972).

From these two figures, to estimate pore pressure is first by plotting logarithmic of resistivity versus depth then plotting the same graph for an interested well. If

plotted points diverge from the normal line, top of overpressured formation is noted at that specific depth (SPE, 1983). At any depth, pore pressure can be found by measuring ratio of extrapolated to observed resistivity then find the fluid pressure gradient corresponding to this ratio (Martin, 1972) and finally fluid pressure gradient is multiplied to depth to find the pore pressure (Hubbert and Rubey, 1959). This process is repeated at various depths.

Based on this method, pressure gradient for a normal environment was found to be 0.465 psi/ft so any deviation higher from this value is called an abnormal pressure (Martin, 1972, SPE, 1983). A case study was performed for this method in determining abnormal pore pressure as per mentioned in a paper written by Evers and Richard, 1983 giving predictions estimated to be 0.03 psi/ft.

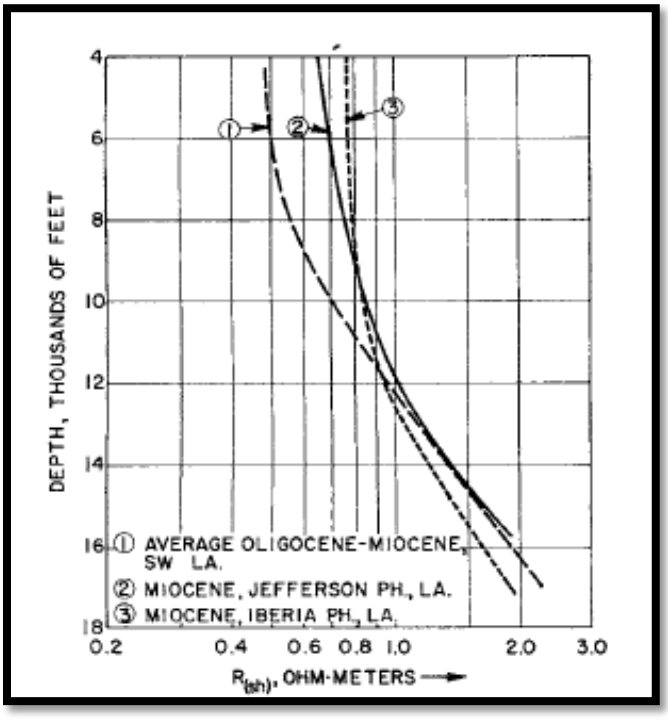

Figure 2.7: Resistivity vs Burial Depth for Normal Pressured (Hottmann and Johnson, 1965)

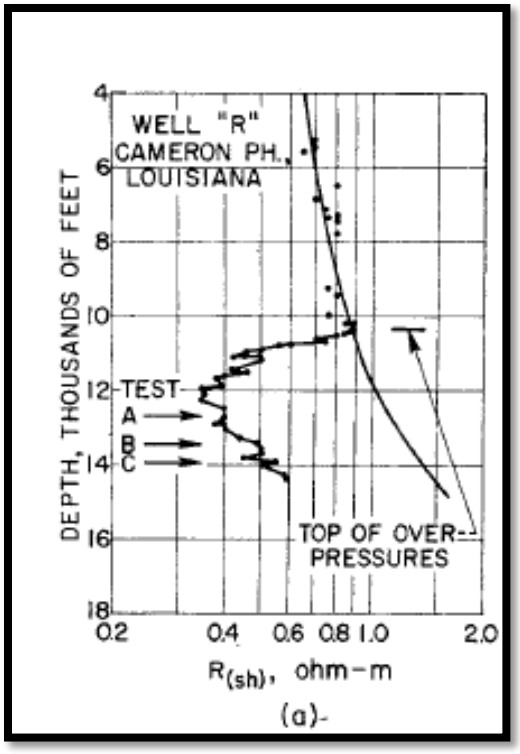

Figure 2.8: Resistivity vs Burial Depth for Abnormal Pressured (Hottmann and Johnson, 1965)

Limitations of both methods include undefined problems in tools (Fertl and Chilingarian, 1977), conditions of borehole and the characteristics of surrounding which affect readings on both resistivity and acoustic logs. Furthermore, it is subjective to find the normal trend which creates problems with no experience regionally and the empirical relationship between pressure gradients and petrophysical parameters are based on data obtained on this regional area (Alixant and Desbrandes, 1991).

Eaton improved that original method by Hottman and Johnson in his 1972 and 1975 papers where he stated that this method is only applicable to Tertiary Age sediments such that abnormal pressure is due to overburden stress (Eaton, 1972). Eaton also used a bigger data base in developing equations relating to pore

pressure to deviation ratio between values of log observed and values from normal trend line (Yoshida, Ikeda and Eaton. 1996), same approach as laid out above.

2.5.2 Electrical Logs

Another paper introduced by Foster, 1966 whereby a different approach was made in the estimation of pore pressure using equations to derive empirically derived methods. Hubbert and Rubey, 1959 derived an **Equation 2.2** relating net overburden pressure to porosity where $ø$ is porosity, $ø_i$ is porosity at surface, σ is net overburden pressure or effective stress and K is a constant. First porosity is determined at that particular depth then overburden pressure is determined assuming there is a normal pressure (Swarbrick, 2001). Then a logarithmic plot of porosity against net overburden pressure (effective stress) is constructed as shown in **Figure 2.9** showing both normal and abnormal trends.

$$ø = ø_i \, e^{-K_\sigma} \qquad \textbf{(2.2)}$$

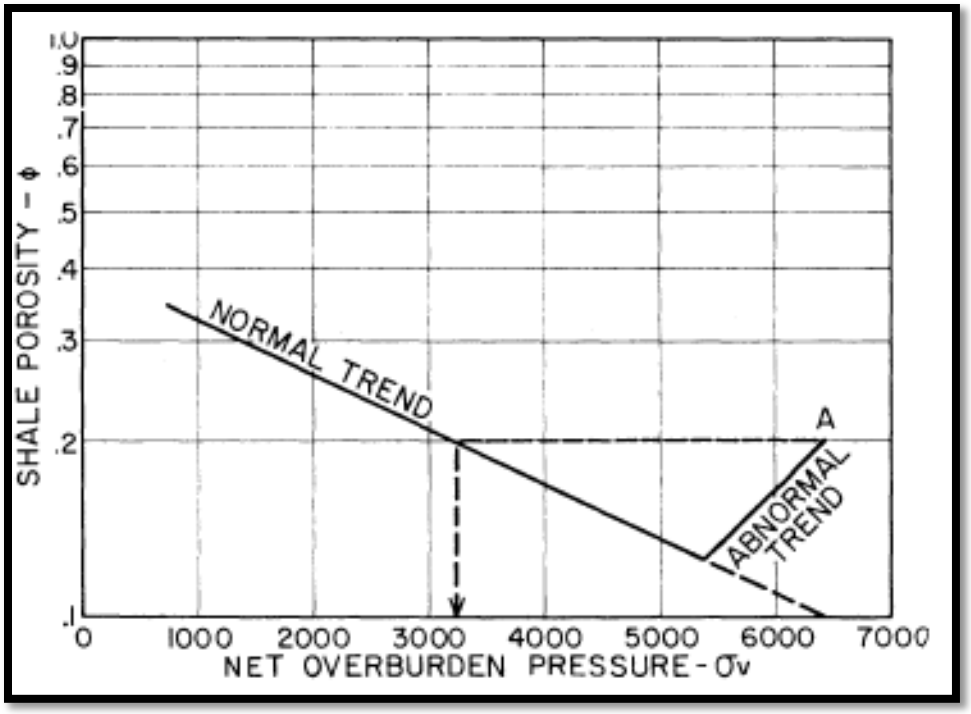

Figure 2.9: Porosity vs Net Overburden Pressure (Foster, 1966)

An electrical survey is done in this case run virtually on borehole through all the drilled sections then formation resistivity factor, *F* (Eaton, 1975) is calculated which is a function of porosity such that it is the ratio of electrical resistivity of rock cube of 100% water saturated, R_s to electrical resistivity of water with saturated cube, R_w as shown in **Equation 2.3** (Eaton, 1972). Archie, 1942 stated that *F* is indirectly proportional to porosity, $ø^m$ where a = 1and a is tortuosity constant and m is cementing factor which usually have values in a range of 1.8 to 2.3 (Holbrook and Hauck, 1987), where porosity decreases so average pore tortuosity increases as shown in **Equation 2.4**.

$$\boldsymbol{F = \frac{R_s}{R_w}} \qquad \textbf{(2.3)}$$

$$\boldsymbol{F = \frac{a}{\emptyset^m}} \qquad \textbf{(2.4)}$$

F when plotted logarithmically with net overburden pressure (effective stress), $\boldsymbol{\sigma}$ will result in a straight line. Using **Equations 2.2 and 2.4** and taking logarithmically gives **Equation 2.5**.

$$\boldsymbol{ln\, F = K\, m\, \sigma - m\, ln\, \emptyset} \qquad \textbf{(2.5)}$$

Simplifying this by plotting *ln F* against depth instead of porosity against net overburden pressure (effective stress), $\boldsymbol{\sigma}$ gives same plot as that shown in **Figure 2.9**. This plot is shown in **Figure 2.10**. For a given value of *F* at that particular depth, find a depth at the straight line for same value of *F* there is. Then calculate net overburden pressure or effective stress, σ using **Equation 2.6** where *D* is depth. Hence pore pressure, *P* is calculated as in **Equation 2.7** (Eaton, 1972) where *S* is overburden pressure which is usually 1.0*D* (Eaton, 1975) and σ is effective stress. Overburden pressure, S is an integral part for bulk densities multiplies by gravitational constant of Earth from surface to that of preferred depth (Holbrook and Hauck, 1987).

Note that, bulk density is a function of lithology and usually obtained from density logs or estimated from seismic data of interval velocity or sonic well logs (Yoshida, Ikeda and Eaton, 1996). Holbrook, Maggiori and Hensley also stated more of this method in detail in 1995 by which they explained this method of application incorporating petrophysical data with the mineralogy in formations through all types of sedimentary rocks.

$$\sigma = 0.535\ D \quad (2.6)$$

$$P = S - \sigma_v \quad (2.7)$$

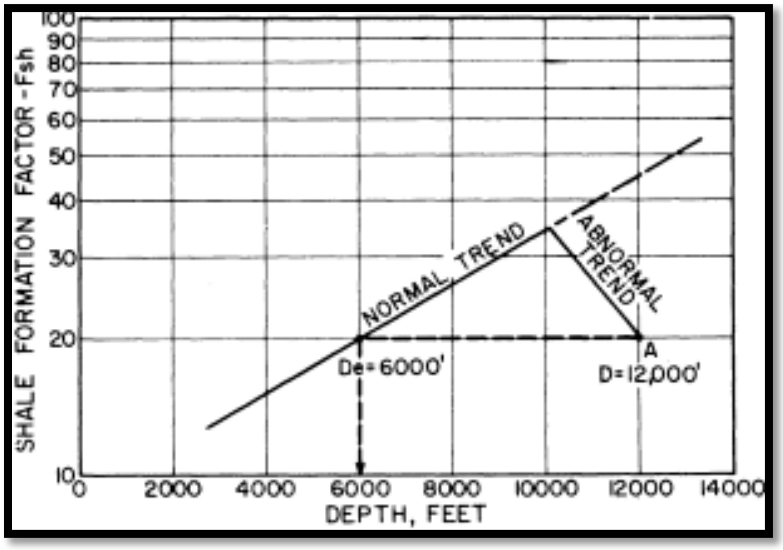

Figure 2.10: Formation Factor vs Depth (Foster, 1966)

Limitations of these methods are such that until a hole has been drilled, electrical surveys is not possible, this pressure estimate method depends on traits of offset well and intermediate logs (Foster, 1966).

2.5.3 Seismic

This is where velocities obtained from seismic are used in predicting pore pressure as explained by Sayers et al. in his 2000 paper. These velocities are smoothed out. **Figure 2.11** shows how transformation of velocity to pore pressure can be done from velocity-depth graph to effective stress-depth graph. This was done by employing different methods by scientists and/or engineers. The velocities are refined to give a better comprehension on the spatial distribution

and magnitude of pore pressure (Sayers, Johnson and Denyer, 2000, Huffman et al., 2011, Tang et al., 2011, Khaksar, 2011). Bowers, 1995 suggested that seismic velocities, *v* are related to effective stress from an **Equation 2.8** below where v_o is the velocity of saturated and unconsolidated sediments and *A* and *B* are constants describing variations in velocities with increasing effective stress, σ (Ji and Fan, 2010):

$$\boldsymbol{v = v_o + A\sigma^B} \qquad \textbf{(2.8)}$$

Then pore pressure can be calculated using **Equation 2.7**. Bowers in his 1995 paper also made full use of this method but extending further by accounting on excess pressure due to under compaction and fluid expansion overpressure (Kelly, Skidmor and Cotton, 2005, Nygaard et al., 2008) mechanisms through definition of curves of unloading and loading respectively (Kulkarni, Meyer and Sixta, 1999). He later made a deeper review and revised method in this matter by cross-plotting sonic velocity with density data due to velocities reversal and to better identify high pore pressure regions (Bowers, 2001).

Sayers and Woodward, 2001 later enhanced this prediction method by using reflection tomography which improved resolution spatially which is important in the design of well incorporating P and S types of waves (compressional and shear respectively). A regional study has been done in the Gulf of Mexico and North Sea implying this method (Cibin et al., 2004) while a case study in South China Sea was done incorporating this method (Cao et al., 2006) and another one in northeast of Sichuan (Yu et al., 2009). A deeper understanding also was applied to a case study done in West Kuwait field (Kumar et al., 2010).

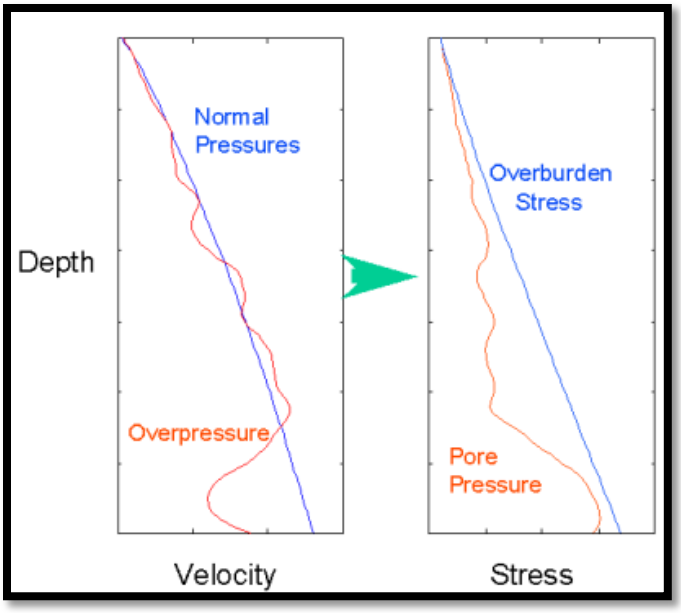

Figure 2.11: Transformation of Velocity to Pore Pressure (Sayers, Johnson and Denyer, 2000)

Limitation of this method is such that equation from unloading curve is not perfect giving lower pore pressure determination but this was later revised by Ji and Fan in their 2010 paper which improved the use of Bower's method as per explained above.

2.5.4 Drilling Data

This is where Bill Rehm in his paper in 1971 laid out the use of drilling equations in the estimation of pore pressure value. This method provides real time or semi-real time information (Fertl and Chilingarian, 1977, Greenwood, Dautel and Russell, 2009). Reasons why this method can work are:

1) When drilling bit is entering the abnormal pressured zone, drilling rate measured is very much related to porosity or density as per mentioned in the previous methods hence pore pressure can be determined.

2) When the difference between wellbore and pore pressure decreases, there is an increase in the rate of drilling denoting that drilling in an abnormal pressured zone has been reached.

The concept employed by this method includes the use of d-equation as main indicator of the difference in pressures as shown in **Equation 2.9** where d is the drilling equation's exponent, *D* is diameter of drilling bit in inch, *N* is the rotary speed in rate per minute, *R* is rate of penetration in feet per hour and *W* is load on bit in pound. These parameters are obtained in real time and are normalised to a set of conditions beforehand (Yoshida, Ikeda and Eaton, 1996).

From this, upon entering the abnormal pressured zone, value of d can be put on trend to keep a constant value in the difference in pressures. Hence bottom hole pressure can be calculated. At any depth, formation pressure gradient is equivalent to the summation of mud weight gradient in normal pressured zone with gradient of the difference in pressures (Rehm and McClendon, 1971, Atashbari and Tingay, 2012).

$$\boldsymbol{d = \frac{log\frac{R}{60N}}{log\frac{12W}{10^6 D}}} \qquad \textbf{(2.9)}$$

Limitations of this method are such it is not possible to develop an equation suitable for all conditions, difficulties in getting constant bit weight, mud weight and rotary speed especially upon entering one zone to another different zone although these values can desirably be changed. However this is such a daunting approach and will only give more confusion as explained by Rehm, 1971.

2.5.5 Flowline Temperature Gradients

This method was suggested by Wilson and Bush, 1973 by which pore pressure determination is done by observing the variations of temperature of mud at surface. Temperature in subsurface increases with depth as given in **Equation 2.10** below where *G* is the geothermal gradient, *D* is depth in feet and *T* is temperature in Kelvin:

$$\boldsymbol{G = 100\frac{T_2 - T_1}{D_2 - D_1}} \qquad \textbf{(2.10)}$$

G is constant at a specific depth of area; higher value of *G* has a relationship with the pore pressure obtained from abnormal pressured region. Theoretically, this departure from normal behaviour is due to heat within earth moving outwards from region of molten solid and then radiates into space. For low conductivity formation, heat increase till the difference in temperature across the formation allows flow of heat in the insulator to be equivalent to flow of incoming heat. Increase in geothermal gradient tells an increase in pressure gradients upon entering an abnormal pressured region as example is shown in **Figure 2.12** where a graph of flowline temperature gradient versus depth is drawn for both normal and abnormal pressured regions (Wilson and Bush, 1973).

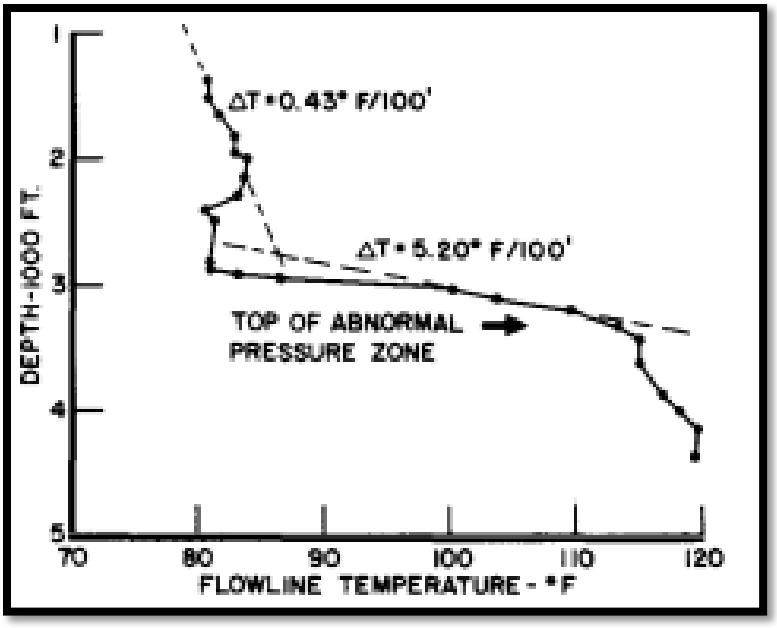

Figure 2.12: Depth vs Flowline Temperature (Wilson and Bush, 1973)

An increase in the value of *G* reflects an increase in temperature so **Equation 2.10** can be rewritten as shown in **Equation 2.11** where ΔT is temperature gradient. So this method can indicate the transition between zones hence pore pressure can be determined quantitatively denoting value of greater flow line temperature gradient or using gradient ratio as shown in **Equation 2.12** where GR is a ratio of abnormal flow line temperature gradient, ΔT_a to normal flow line temperature gradient, ΔT_n.

$$\boldsymbol{\Delta T = 100 \frac{T_2 - T_1}{D_2 - D_1}} \qquad \textbf{(2.11)}$$

$$\boldsymbol{GR = \frac{\Delta T_a}{\Delta T_n}} \qquad \textbf{(2.12)}$$

Analysing the value of *GR* will determine the value for pore pressure as given in **Figure 2.13** where a graph of gradient ratio versus pore pressure is drawn for a normal pressured region.

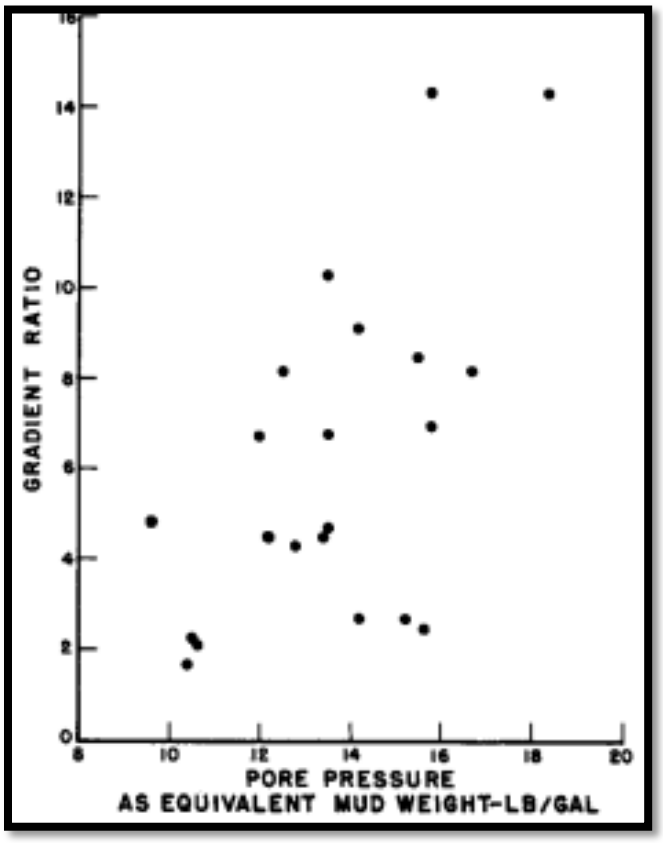

Figure 2.13: Gradient Ratio vs Pore Pressure (Wilson and Bush, 1973)

Limitations of this method are such that materials within the grains do not have the same thermal traits, flow line temperature can be greatly affected by certain factors and a lot of assumptions must be considered.

2.6 Highlights of Literature Reviews

It was found that there are many different types of pores and their classifications corresponding to different porosities and other properties. There seems to be a relationship between pore types, their classifications with pore pressure. Secondly, it was found that there are many different types of pressures corresponding to different geological settings and mechanisms producing. Finally different methods in predicting pore pressure were laid out and briefly described and compared. This clearly established the specific findings in all previous studies in relation from pore types, their classifications with pore pressure and its estimation technique.

Chapter 3 METHODOLOGY

3.1 Project Activities, Timeline and Tools

The diagram **Figure 3.1** below shows an outline of activities done in this project and the next **Table 3.1** shows a Gantt chart of project timeline.

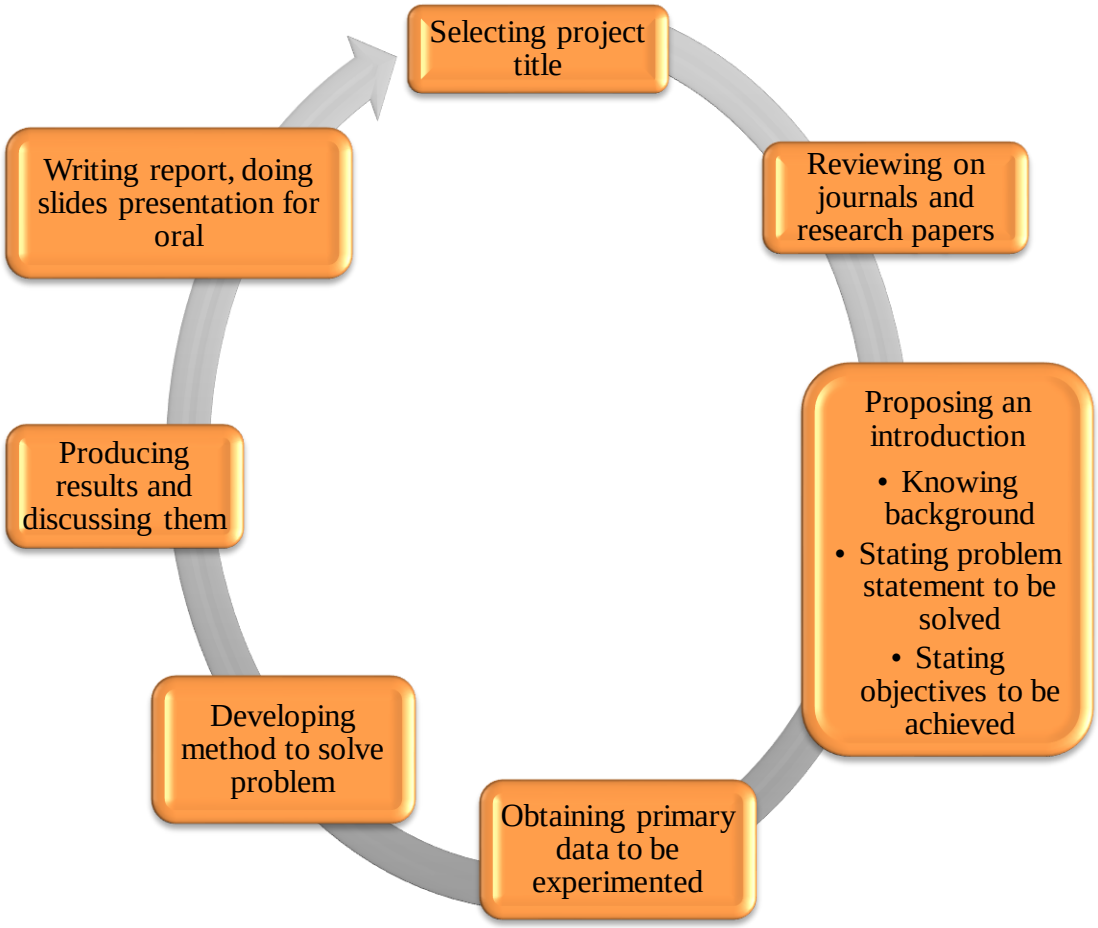

Figure 3.1: Outline of Activities

Primary data was given which includes core and geological data, which was already gathered from Azar Sarvak field in Iran. A method of critical evaluation and reviews were made on each journal paper found. A collection of journals

papers were reviewed chronologically, denoting amendment made between studies of pore types and their classifications with pore pressure, and the advances of each approach with time in predicting pore pressure. With these two vital elements, problems could then be solved.

Table 3.1: Gantt Chart of Project Timeline

Research Components		Months																
		March - April							April - May						May - June			
		Week																
		1	2	3	4	5	6	7	8	9	10	11	12	13	14	15	16	17
1	Chose Project Title																	
2	Commencement of Project Work and Project Writing in Introduction and Literature Review																	
3	Progress Report Submission																	
4	Draft Report 1 Submission																	
5	Project Writing in Methodology, Results and Conclusions																	
6	Draft Report 2 Submission																	
7	Spiral Bound Submission																	
8	Make Slides Presentation																	
9	Oral Presentation																	
10	Hard Bound Submission																	

Details of pore types, their classifications with pore pressure estimation techniques are shown in previous sections. This methodology is based on manipulation of literatures done from published works such as journals, books and websites. The diagram **Figure 3.2** below shows a flowchart of step-by-step procedure how the main activities had been carried out to get the results in the next section.

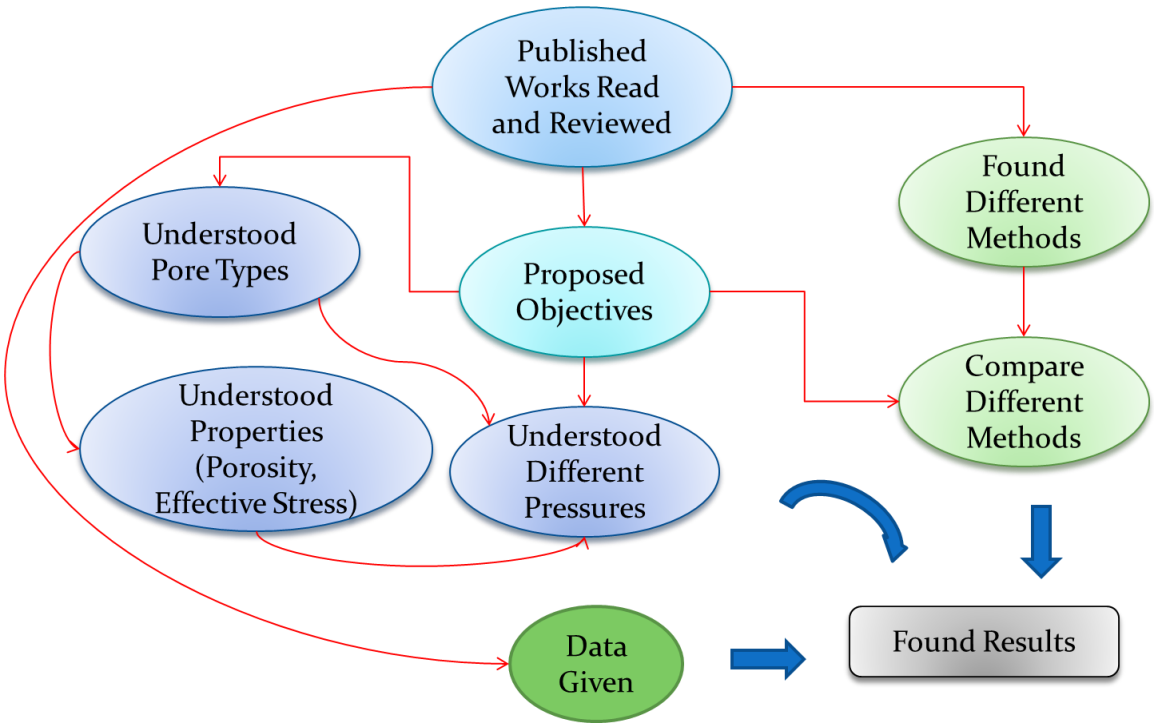

Figure 3.2: Flowchart of Step-by-step Procedure

1. A full set of about 120 published works were obtained mainly in the form of journals, books and certified websites. First the soft copies were all renamed in accordance to the year it was published. Then each of this paper from the old to a new one was read and reviewed critically, making sure which made a huge impact on the proposed objectives.
2. From the papers read, pore types and their classifications could finally be understood then they also have different properties like porosities and effective stresses they rely on, which in turn give different pore pressures.
3. The correlation between pore types, their classifications was established to that of pore pressures.
4. From this, each paper was also reviewed on approaches made to actually calculate pore pressure. Different approach was compared and contrasted, noted the advantages, disadvantages, limitations and assumptions.

5. A set of core and geological data was given beforehand this project, these were read and analysed if it could be applied to the project itself within a time constraint given. These data were obtained from Azar Sarvak field in Iran, consisting of explanations of layer of different zones prevailing different lithology while core data was that obtained from a specific depth to determine permeability. A correlation figure was also given between this property to porosity.
6. These three main elements produced results that will be discussed next in detail.

Chapter 4 RESULTS AND DISCUSSIONS

4.1 Data Gathering and Critical Discussions

As said, since this project is mostly research literature based, to finally understand the relationship between pore types, their classifications with pore pressure; only core and geological data were given to comprehend about it further as in the **Appendices** section. Both of these data were obtained from an existing field in Azar Sarvak in Iran where each layer of different zones was established prevailing different lithology and petrophysical properties. A result of core analysis obtained from a certain depth was analysed in obtaining rock properties such as permeability and correlation of this property with porosity was made. Please refer **Appendix A** and **Appendix B** for more detail descriptions on these data. However these appendices were not able to support information on this project study, probably in the future as recommended in next section.

Pore Type Classification:

It was found that for a different pore type there is a specific value of porosity. There were three different basic types of porosities found: stiff, reference and crack pore. These different pore types and their classifications have aspect ratio of 0.7-0.8, 0.12-0.15 and 0.01-0.02 respectively. It was proven that the digenetic history affected the minerals and fluids within the rocks hence affect the type of pore therein. This result is shown on **Table 4.1**.

Table 4.1: Different Pore Types

Pore Types		
Stiff	Reference	Cracks
0.7-0.8	0.12-0.15	0.01-0.02

Porosity and Other Parameters:

Firstly, it was found porosity is a function of different parameters. It is interrelated to pore size (pore geometry and type). Pore size on the other hand is also related to how particles are sorted making up rock fabric hence its relationship to porosity. Depending how grains are packed, porosity is between 0.26 to 0.48. For sand grains of different sizes, ø is between 0.30 to 0.35. This is because if irregularities in shape increase, gaps are getting bigger thus giving bigger porosity. This relates to the PSD. PSD is denoted by effective radius of pore body. It also plays an important role in controlling the structure of pore types.

Secondly, note also that porosity is a function of an effective stress and it will greatly affect the values of porosity. Effective stress may differ between pore types that of sandstone and chalk due to differential effect in the spherical pores in chalk and slot porosity in that of sandstones. The latter tends to have effective stress approximately closer to unity.

Thirdly, a correlation of velocity and porosity was found for different pore types and their classifications. Geological processes such as dolomitisation, dissolution and cementation in the pores are the main factors affecting porosities and how velocities are different for each pore type. In other words, the spatial distributions of variation in pore types and their classifications are due to the effect of these processes and their effects towards other petrophysical properties like porosities. Velocity is more affected in stiff pores than in crack pores because shear wave (S-wave velocity) is more affected by cracks than stiff pores (Luanxiao et al., 2013, Irineu and Roseane, 2012). The relationship between porosity and these parameters is shown on **Figure 4.1**.

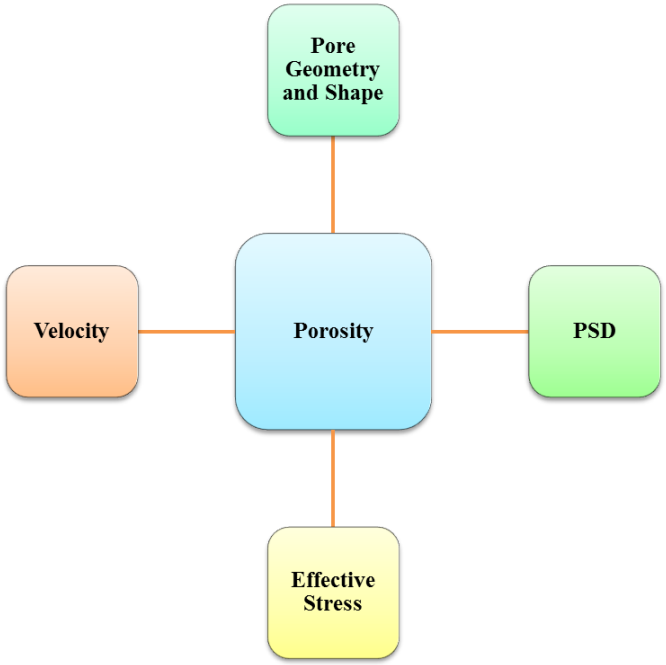

Figure 4.1: Relationship between Porosity and Other Parameters

Porosity and Pore Pressure:

It was noted that porosity-effective stress relationship is the one majorly used in determining pore pressure. After getting hands-on in a full set of published works such as journals as in the literature reviews, it can be finally said that there is indeed a relationship between pore types, their classification with pore pressure, rather indirectly as per explained in **Figure 4.2**:

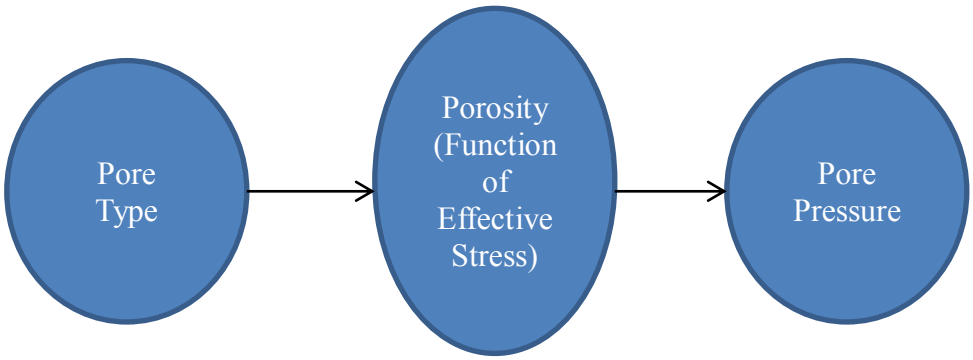

Figure 4.2: Relationship of Pore Type with Pore Pressure

Pore Pressure and Prediction Methods

Since correlation was proven to exist, now different methods as per briefly explained in literature reviews were compared and contrasted denoting the differences between them, limitations and assumptions used on each. Note that, this prediction method is improving with time and assumptions are based on different environmental and geological settings. Firstly, different method is divided into two types: argillaceous and permeable formation approach. As stated first approach makes full use the porosity-effective stress relationship while the second approach is a direct observation on pore pressure. Since focus is more towards in the pre-drilling phase as to find pore pressure so drilling activities can be performed at an ease, so only argillaceous type of approach is used. The result is as shown on **Table 4.2**.

Table 4.2: Different Prediction Methods

Method	**Resistivity and Acoustic**	**Electrical Logs**	**Seismic**	**Drilling Data**	**Flowline Temperature Gradients**
Type	Argillaceous			Permeable Formation	
Obtain Period	Pre-drilling			During drilling	
Yes/No	Yes			No	

In addition, limitations of each method are as presented in **Table 4.3**. This helped in narrowing down further on each method. Note that this includes cost, time, risk and if it is easily obtainable.

Table 4.3: Limitations of Each Method

Limitations of Each Method				
Resistivity and Acoustic	**Electrical**	**Seismic**	**Drilling Data**	**Flowline Temperature Gradients**
• Problems in tools • Conditions of borehole • Traits of surrounding which affect readings	• Until a hole has been drilled, electrical surveys is not possible • Depends on traits of offset well and intermediate logs.	• Equation from unloading curve is not perfect giving lower pore pressure determination	• Impossible to develop an equation suitable for all conditions • Difficulties in getting constant bit weight, mud weight and rotary speed	• Materials within the grains do not have the same thermal traits, flow line temperature can be greatly affected. • Make a lot of assumptions!

From this, a critical evaluation of different methods and analysis in a specific environment are needed for this to be more proven, where the best method is applied. It was found that the first method that is combination of logs of electrical with resistivity and acoustic was the best method to be applied since these data could be easily obtained from the existing field. However, these logs data required time to obtain. So this study is left for future research to be done. Seismic is not used among those three stated above because of its extensive limitation and of course due to its expensive cost of procedure.

If justifications made on these results and combination of data was present, this can be done like so:

1. Obtain electrical logs such as resistivity, sonic, gamma ray in different intervals.
2. Plot sonic logs of different intervals together where points are smoothed to see them visibly and reading points are averaged.
3. Align sonic with gamma ray logs (along with other logs like resistivity) in determining tops of lithology and formation analysis in different zones by observing any sudden changes from general trend based on own geological interpretation.
4. Identify between sand and shale zones using gamma ray logs and obtains volume of shales at each point of interest.
5. For each point of interest, find the corresponding hydrocarbon and non-hydrocarbon bearing zones and find velocity from sonic log.
6. An accurately calibrated velocity curve is plotted logarithmically for a continuous trend line in all intervals.
7. Determine pore pressure using known method mainly that one that utilises Eaton's approach (as explained in literature review). Why? Because it is famously known to be universal in Oil and Gas Industry.
8. Modify results for different pressure points.

The detail of how sonic/acoustic and electrical logs can be read as laid out in literature review.

Chapter 5 CONCLUSIONS AND RECOMMENDATIONS

5.1 Conclusions

Highlighting the most significant findings as per examined in the previous sections, that is there is indeed an indirect relationship between pore types, their classifications with pore pressure. However this relationship cannot be mathematically expressed. Moreover, different approaches of pore pressure prediction were understood and identified and each of this method was discussed in detail and a best method is chosen.

5.2 Future Recommendations

Perhaps with more time on hand, other researchers may continue this research by providing experimental approach on this subject to a few case studies. By which this can be done by having more data such as offset log data, core and geological data so the relationship can be more vividly proven. Seismic will probably give better results but considering the factor in economy and time and the fact it is in an early stage of development plan, it is indeed very expensive method and merely time consuming. Hence, the availability of log is enough and will be processed in relation to the available core and geology data as in the **Appendices**, in producing output as such to prove the relationship of pore types, their classifications with pore pressure so the reports of **Appendices** can support this research study (of course estimation is built on several assumptions).

Note that pore pressure prediction has improved with time. Software has been used in prediction nowadays with the sophistication of parameters applied. This is done by relating pore pressure and fracture gradients with appropriate model of

known method such as Eaton's using sophisticated integrated computer software. Some environmental settings use advanced tools such as MWD and LWD. These tools and approaches stated have the ability of getting real time information. Moreover, it can provide information on wellbore stability and evaluate stress fields of wellbore.

In the future, it is also recommended that processes producing different pore pressure become a focal point in order to provide better interpretation of large amount of data. In addition, uncertainties associated with any methods used should be properly calibrated allowing more reliable predictions.

REFERENCES

1. Alixant, J.-L., & Desbrandes, R. (1991, September 1). Explicit Pore-Pressure Evaluation: Concept and Application. Society of Petroleum Engineers. doi:10.2118/19336-PA.

2. Atashbari, V., & Tingay, M. R. (2012, January 1). Pore Pressure Prediction in Carbonate Reservoirs. Society of Petroleum Engineers. doi:10.2118/150835-MS.

3. Bowers, G. L. (1995, June 1). Pore Pressure Estimation From Velocity Data: Accounting for Overpressure Mechanisms Besides Under compaction. Society of Petroleum Engineers. doi:10.2118/27488-PA.

4. Bowers, G. L. (2001, January 1). Determining an Appropriate Pore-Pressure Estimation Strategy. Offshore Technology Conference. doi:10.4043/13042-MS.

5. Cao, S., Xie, Y., Liu, C., Yan, G., YI, P., Cai, J., & XU, L. (2006, January 1). Multistage Approach on Pore Pressure Prediction - A Case Study in South China Sea. Society of Petroleum Engineers. doi:10.2118/103856-MS.

6. Christina Marie Dicus (2007, December), Relationship between Pore Geometry, Measured by Petrographic Image Analysis, and Pore-Throat Geometry calculated from Capillary Pressure as a means to predict Reservoir Performance in Secondary Recovery Programs for Carbonate Reservoirs. MSc Geology, Texan A&M University.

7. Cibin, P., Martera, M. D., Buia, M., Calcagni, D., Runcer, D. J., & Talkan, T. (2004, January 1). What Seismic Velocity Field For Pore Pressure Prediction? Society of Exploration Geophysicists.

8. Contreras, O. M., Hareland, G., & Aguilera, R. (2011, January 1). An Innovative Approach for Pore Pressure Prediction and Drilling Optimization in an Abnormally Sub pressured Basin. Society of Petroleum Engineers. doi:10.2118/148947-MS.

9. Eaton, B. A. (1972, August 1). The Effect of Overburden Stress on Geopressure Prediction from Well Logs. Society of Petroleum Engineers. doi:10.2118/3719-PA.

10. Eaton, B. A. (1975, January 1). The Equation for Geopressure Prediction from Well Logs. Society of Petroleum Engineers. doi:10.2118/5544-MS.

11. Fertl, W. H., & Chilingarian, G. V. (1977, April 1). Importance of Abnormal Formation Pressures (includes associated paper 6560). Society of Petroleum Engineers. doi:10.2118/5946-PA.

12. Foster, J. B. (1966, February 1). Estimation of Formation Pressures From Electrical Surveys-Offshore Louisiana. Society of Petroleum Engineers. doi:10.2118/1200-PA.

13. Greenwood, J. A., Dautel, M. R., & Russell, R. B. (2009, January 1). The Use of LWD Data for the Prediction and Determination of Formation Pore Pressure. Society of Petroleum Engineers. doi:10.2118/124012-MS.

14. Gutierrez, M. A., Braunsdorf, N. R., & Couzens, B. A. (2006, January 1). Evaluation, Calibration, And Ranking of Pore Pressure Prediction Models. Society of Exploration Geophysicists.

15. Hamouz, M. A., & Mueller, S. L. (1984, January 1). Some New Ideas for Well Log Pore-Pressure Prediction. Society of Petroleum Engineers. doi:10.2118/13204-MS.

16. Haugland, M., Zhang, J., Sarker, R., Axon, A., Azbel, K., Wilhelm, R., … Zhang, I. (2013, March 26). Pore Pressure Prediction in Unconventional Resources. International Petroleum Technology Conference. doi:10.2523/16849-MS.

17. Haugland, S. M., & Tichelaar, B. W. (2008, January 1). Cation Exchange Capacity Effects On Resistivity-Based Pore Pressure Predictions. Society of Petrophysicists and Well-Log Analysts.

18. Holbrook, P. W. (1989, January 1). A New Method for Predicting Fracture Propagation Pressure From MWD or Wireline Log Data. Society of Petroleum Engineers. doi:10.2118/19566-MS.

19. Holbrook, P. W., & Hauck, M. L. (1987, January 1). A Petrophysical-Mechanical Math Model for Real-Time Wellsite Pore Pressure/Fracture Gradient Prediction. Society of Petroleum Engineers. doi:10.2118/16666-MS.

20. Holbrook, P. W., Maggiori, D. A., & Hensley, R. (1995, December 1). Real-Time Pore Pressure and Fracture Gradient Evaluation in All Sedimentary Lithologies. Society of Petroleum Engineers. doi:10.2118/26791-PA.

21. Hottmann, C. E., & Johnson, R. K. (1965, June 1). Estimation of Formation Pressures from Log-Derived Shale Properties. Society of Petroleum Engineers. doi:10.2118/1110-PA 2.

22. Hubbert, M. King, and Rubey, W. W., 1959, Role Of Fluid Pressure In Mechanics Of Over thrust Faulting, Part 1, Geological Society of America GSA Bulletin, February, 1959, p 70ff.

23. Huffman, A. R. (2001, January 1). The Future of Pore-Pressure Prediction Using Geophysical Methods. Offshore Technology Conference. doi:10.4043/13041-MS.

24. Huffman, A. R., Meyer, J. S., Gruenwald, R. M., Buitrago, J., Suarez, J., Diaz, C., … Dessay, J. (2011, January 1). Recent Advances in Pore Pressure Prediction in Complex Geologic Environments. Society of Petroleum Engineers. doi:10.2118/142211-MS.

25. Irineu de A. Lima Neto and Roseane M. Missagia (2012, January 30). Elastic Properties including Pore Geometry Effect on Carbonates: A Case Study of Glorieta-Paddock Reservoir at Vacuum Field, New Mexico.

26. J. R. Nimmo. (2004). Porosity and Pore Size Distribution. U.S. Geological Survey, Menlo Park, CA 94025, USA.

27. Ji, R., & Fan, H. (2010, January 1). Improvement and Application of Bowers. Society of Petroleum Engineers. doi:10.2118/131199-MS.

28. Jones, P. H. (1969, July 1). Hydrodynamics of Geopressure in the Northern Gulf of Mexico Basin. Society of Petroleum Engineers. doi:10.2118/2207-PA.

29. Kelly, M. C., Skidmor, C. M., & Cotton, R. D. (2005, January 1). Pressure Prediction For Large Surveys. Society of Exploration Geophysicists.

30. Khaksar, A. (2011, January 1). Depth Limit of Velocity-Effective Stress Relationships For Pore Pressure Prediction, Implications For Wellbore Stability Analysis. American Rock Mechanics Association.

31. Khan, M., Teufel, L. W., & Zheng, Z. (2000, January 1). Determining the Effect of Geological and Geomechanical Parameters on Reservoir Stress path through Numerical Simulation. Society of Petroleum Engineers. doi:10.2118/63261-MS.

32. Khazanehdari, J. (2012, January 1). Pore Pressure Prediction Challenges in the Middle East Region. Society of Petroleum Engineers. doi:10.2118/162276-MS.

33. Kulkarni, R., Meyer, J. H., & Sixta, D. (1999, January 1). Are Pore Pressure Related Drilling Problems Predictable? The Value of Using Seismic Before And While Drilling. Society of Exploration Geophysicists.

34. Kumar, R., Al-Saeed, M. A., Al-Kandiri, J. M., Verma, N. K., & Al-Saqran, F. (2010, January 1). Seismic Based Pore Pressure Prediction In a West Kuwait Field. Society of Exploration Geophysicists.

35. Lane, R. A., & Macpherson, L. A. (1976, September 1). A Review of Geopressure Evaluation From Well Logs - Louisiana Gulf Coast. Society of Petroleum Engineers. doi:10.2118/5033-PA.

36. Lesage, M., Hall, P., Pearson, J. R. A., & Thiercelin, M. J. (1991, June 1). Pore-Pressure and Fracture-Gradient Predictions. Society of Petroleum Engineers. doi:10.2118/21607-PA.

37. Luanxiao Zhao, Mosab Naseer and De-hua Han (2013, January). Quantitative geophysical pore-type characterization and its geological implication in carbonate reservoirs. Geophysical Prospecting. doi:10.1111/1365-2478.12043.

38. Lucia, F. J. (2007, Hardcover), Carbonate Reservoir Characterisation, An Integrated Approach. ISBN: 978-3-540-72740-8.

39. Martin, G. B. (1972, January 1). Abnormal High Pressure and Environment of Deposition. Society of Petroleum Engineers. doi:10.2118/3846-MS.

40. Nygaard, R., Karimi, M., Hareland, G., & Munro, H. B. (2008, January 1). Pore-Pressure Prediction in Over consolidated Shales. Society of Petroleum Engineers. doi:10.2118/116619-MS.

41. Prediction of Abnormal Pressures in Wyoming Sedimentary Basins Using Well Logs. (1983, January 1). Society of Petroleum Engineers. doi:10.2118/11859-MS.

42. Proehl, T. S. (1994, January 1). Pore Pressures, Fracture Gradients, and Drilling Economics. Society of Petroleum Engineers. doi:10.2118/27493-MS.

43. Rehm, B., & McClendon, R. (1971, January 1). Measurement of Formation Pressure from Drilling Data. Society of Petroleum Engineers. doi:10.2118/3601-MS.

44. Sayers, C. M., & Woodward, M. J. (2001, January 1). Enhanced Seismic Pore-Pressure Prediction. Offshore Technology Conference. doi:10.4043/13044-MS.

45. Sayers, C. M., Johnson, G. M., & Denyer, G. (2000, January 1). Predrill Pore Pressure Prediction Using Seismic Data. Society of Petroleum Engineers. doi:10.2118/59122-MS.

46. Scott, D., & Thomsen, L. A. (1993, January 1). A Global Algorithm for Pore Pressure Prediction. Society of Petroleum Engineers. doi:10.2118/25674-MS.

47. Shafer, J. L., Boitnott, G. N., & Ewy, R. T. (2008, January 1). Effective Stress Laws For Petrophysical Rock Properties. Society of Petrophysicists and Well-Log Analysts.

48. Shaker, S. S. (2002, January 1). Predicted vs. Measured Pore Pressure: Pitfalls and Perceptions. Offshore Technology Conference. doi:10.4043/14073-MS.

49. Smith, J. R. (2000, January 1). Case History of Integrating Multisource Data for Pore Pressure Prediction. Society of Petroleum Engineers. doi:10.2118/59228-MS.

50. Swarbrick, R. E. (2001, January 1). Pore-Pressure Prediction: Pitfalls in Using Porosity. Offshore Technology Conference. doi:10.4043/13045-MS.

51. Syngaevsky, P. E. (2001, January 1). Pore pressure and fracture pressure analyses in non-consolidated rocks. American Rock Mechanics Association.

52. Tang, H., Luo, J., Qiu, K., Chen, Y., & Tan, C. P. (2011, January 1). Worldwide Pore Pressure Prediction: Case Studies and Methods. Society of Petroleum Engineers. doi:10.2118/140954-MS.

53. Vernik, L. (2011, January 1). Unified Model For Continuous Pore Pressure Prediction In Shale. American Rock Mechanics Association.

54. Warpinski, N. R., & Teufel, L. W. (1992, June 1). Determination of the Effective-Stress Law for Permeability and Deformation in Low-Permeability Rocks. Society of Petroleum Engineers. doi:10.2118/20572-PA.

55. Weakley, R. R. (1990, January 1). Determination Of Formation Pore Pressures In Carbonate Environments From Sonic Logs. Petroleum Society of Canada. doi:10.2118/90-09.

56. Weakley, R. R. (1990, January 1). Plotting Sonic Logs To Determine Formation Pore Pressures and Creating Overlays To Do So Worldwide. Society of Petroleum Engineers. doi:10.2118/19995-MS.

57. Wilson, G. J., & Bush, R. E. (1973, February 1). Pressure Prediction with Flowline Temperature Gradients. Society of Petroleum Engineers. doi:10.2118/3848-PA.

58. Yan, F., Han, D., & Ren, K. (2012, November 4). A New Model for Pore Pressure Prediction. Society of Exploration Geophysicists.

59. Yao, Q., & Han, D. (2009, January 1). Effect of Compaction History On Pore Pressure Prediction. Society of Exploration Geophysicists.

60. Yoshida, C., Ikeda, S., & Eaton, B. A. (1996, January 1). An Investigative Study of Recent Technologies Used for Prediction, Detection, and Evaluation of Abnormal Formation Pressure and Fracture Pressure in North and South America. Society of Petroleum Engineers. doi:10.2118/36381-MS.

61. Yu, W., Jing, P., Zhu, W., Li, Z., Zhang, S., & Qu, Z. (2009, January 1). Abnormal Pore Pressure Prediction of Complex Structure In Northeast of Sichuan. Society of Exploration Geophysicists.

62. Zhang, J., Standifird, W. B., & Lenamond, C. (2008, January 1). Casing Ultra deep, Ultra long Salt Sections in Deep Water: A Case Study for Failure Diagnosis and Risk Mitigation in Record-Depth Well. Society of Petroleum Engineers. doi:10.2118/114273-MS.

APPENDICES

APPENDIX A – Geology Data

Asmari Formation (2782 – 2845.5m MD) – Limestone and minor anhydrite
Kalhur Formation (2845.5 – 3077) - Anhydrite, salt, claystone, minor marl, dolomite and limestone.
Pabdeh Formation (3077 – 3514m MD) – Marl alternating with limestone and rare shale and claystone.
Gurpi Formation (3514 – 3915m MD) – Limestone alternating with marl and minor claystone and trace of shale.

Bangestan Group (3915 – 4762m MD)
Ilam Formation (3915 – 4052m MD) – Limestone with minor marl and claystone.
Surgah / Laffan Formation (4052 – 4059m MD) – Argillaceous Limestone.
Sarvak Formation (4059 – 4668m MD) – Limestone with rare marl.and dolomite.
Kazhdumi Formation (4668 – 4762m MD) – Limestone with minor marl

2.2.2 Lithological description

2.2.2.1 Fars Group

Fars Group originally divided into three formations, in the Azar-2 area the Fars Group consists of two formations, Agha Jari and Gachsaran Formation. with the Bakhtiari Formation missing due to erosion, but is present on the eastern flank of the Azar anticline.

Agha Jari Formation (0-1941 m)

Displays mostly red marl interbedded with sandstone and siltstone layers. Anhydrite/Gypsum layers The Gypsum layer and grey marl increase toward the base of the Formation.
The sandstones are variably consolidated and generally light to dark brown, pale yellow brown-pale red brown and light olive grey, fine to medium grained, generally fine grained, rarely coarse grained, generally well sorted and dominated by sub-angular to sub-rounded quartz grains, loose, friable to moderately hard, slightly calcareous cemented and with traces of mafic minerals.
The siltstones are pale reddish brown to greyish red and moderate red brown, locally argillaceous, calcareous and trace micro micaceous, minor grading to very fine sandstone and rarely grading silty Marl.
The marls are moderate red brown, moderate brown and pale red brown, , generally sticky, soft to firm and locally slight silty and locally very low calcareous grading to claystone.
The claystones are pale yellowish brown, greyish brown, moderate to dark brown, generally soft, sticky and amorphous, locally slight calcareous grading marl, generally non silty and occasionally mottled.

Gachsaran Formation (1941-2782 m)

Comprises of anhydrite interbedded with marl, claystone and salt Beds of variable thickness. This Formation in type section is consists of 7 members, but it was almost impossible to separate all members due to red marls replace most of grey marl, particularly for the first three members (Member 7, 6 & 5) and therefore a well defined sub-devision is not possible.

Member 7-4 (1941-2251 m)

Mostly consists of anhydrite layers and red marl interbedded with grey marl and some limestone beds. The top Gachsaran is picked at the first appearance of an approcimately 1 m thick anhydrite bed.

Member 4 (2251-2590 m)

Mostly consists of anhydrite and salt layers interbedded with Marl and claystone.The top is picked at the first appearance of a well defined salt bed.

Member 3 (2590-2718m)

Mostly consists of anhydrite alternative with claystone and some salt beds and thin limestone beds.The top is picked at the base of the last salt bed overlying a thick series of beds with mainly anhydrite and marls.

Member 2 (2718-2752 m)

It comprises of thick salt sequence and a red brown to pale brown marl bed in middle of salt. In Azar-2, a dark reddish brown to dusky red claystone reported in middle of salt sequence. The top is picked at the first appearance of a well defined thick basal salt bed overlying the Cap Rock sequence.

Member 1, Cap Rock (2752-2782m)

Mostly consists of anhydrite interbedded with marl, claystone and some limestone, dolomite or dolomitic limestone. The top is picked at the first appearance below the salt of a thin**, ,** but well defined anhydrite bed (KeyBed A).

2.2.2.2 Undefined Group

Asmari Formation (2782-2845.5 m)

Displays mostly by light grey, medium light grey and light olive grey dolomitic limestone with minor dolomite, anhydrite and claystone.

Kalhur Formation (2845.5-3077 m)

It consists of anhydrite, dolomite, limestone, claystone and minor marl in upper part and salt with trace of anhydrite, marl and limestone in middle part and massive anhydrite with two dolomite / limestone beds in lower part. The Operculina limestone and Basal Anhydrite makes up the lower most part of Kalhur Member. Based on cutting samples and wire line logging data, the Kalhur Member can be divided into 5 different sub members:

Upper Kalhur (2845.5-2888.5m)

It consists of pale yellowish brown, light olive grey, olive grey and dark yellowish brown argillaceous limestone, pale yellowish brown, medium grey to medium dark grey dolomite, dark green grey to olive grey claystone and white-off white microcrystalline to crystalline anhydrite.

Salt Sequence (2888.5-3001m)

It's mainly comprised of coarse crystalline transparent-milky anhydritic salt with trace of anhydrite, limestone and marl. Good to week oil shows reported in some of limestone cutting chips in this sub member. A well defined repea section of the Salt and Massive anhydrite sequence is seen in the well.

Massive Anhydrite (3001-3038m)

This part of Kalhur Member is a thick anhydrite / gypsum layer with a few thin limestone / dolomite beds. Limestone with olive grey, brownish grey, medium dark grey colors are mainly argillaceous and anhydritic. Dark yellowish brown-brown grey dolomite generally is slight argillaceous and highly anhydritic.

Operculina Limestone (3038-3068.5m)

It consists of dark green grey, med dark grey to pale brown marl alternating with limestone. Limestone with a color of buff, light grey and pale yellowish brown is fossiliferous and contain Operculina sp., Echinoid debris, Ostracods and globigerina sp. The fractured limestones are the origin of the high pressure water flow observed while drilling the 12 ½ " section.

Basal Anhydrite (3068.5-3077m)

This part of sequence is entirely comprised of anhydrite and is a regional marker both in Western Iran and in Iraq.

Pabdeh Formation (3077-3514 m)
It comprises of dark green grey, medium dark grey and olive grey marl and marly limestone mostly with basinal pelagic fauna in upper part of the formation. Slightly silty to silty pale brown, dark yellowish brown and brown grey marl/claystone with rare disseminated micro pyrite, minor buff to yellowish grey limestone and dark green grey to dark grey shale at the middle of section. Toward the base carbonate percentage increases, carbonates are mostly yellowish grey, pale yellowish brown, buff to off white, moderate hard to hard, generally argillaceous, glauconitic, cherty and rarely pyritic limestone. Two distinctive moderate brown Marl layers recognized as key beds in upper part of Pabdeh Formation. This Formation can informally be divided into 7 different members based on outcrop studies as follows:

Green marl member (3077-3210m)
This member is upper most part of Pabdeh Formation and overlain by Asamri Formation (Basal Anhydrite). It mainly consists of dark green grey, green grey and olive grey marl that is generally slightly silty, in partly pyritic and locally highly calcareous grading to argillaceous limestone and light grey, medium light grey to pale yellowish brown limestone which is mainly chalky, argillaceous and contain pelagic facies. Two distinctive brown marl layers reported at 3107m and 3124m depth and could be consider as key marker beds. These key beds are about 37m and 54m below the top of the Formation respectively.

Platy limestone member (3210-3260m)
This member with very light grey, light grey to light olive grey color separates Brown bituminous member from Green marl member.

Brown bituminous shale and marl member (3260-3355.5m)
It consists of pale brown, dark brown and dark yellowish brown marl which in partly contain disseminated micro pyrite and locally grading to claystone with trace of buff to light yellowish argillaceous limestone and dark grey to medium dark grey shale. Higher drilling gas values were observed when drilling this unit and may indicate some source rock potential.

Marly limestone member (3355.5-3385m)
This member is mainly comprised of light olive grey, yellowish grey, light grey argillaceous limestone with trace of pale yellowish brown to yellowish grey marl. A two meters thick dark brown to brownish grey claystone with emerald glauconite laid in lower most part of member and can be consider as key bed in next wells.

Cherty limestone member (3385-3460m)
Is mainly consists of light grey, pale yellowish brown and rarely off white moderate hard to hard limestone with chert nodules and minor dark yellowish brown to brownish grey marl and rare dark green grey shale. Toward the base of member, marl percentage increases and color changes to medium grey to greenish grey.

Grey marl and shale member (3460-3476m)
Consists of glauconitic light grey, medium grey to greenish grey marl interbedded with thin bedded very light grey to off white argillaceous limestone. This member separates thin laminated Cherty limestone from Purple shale member.

Purple shale member (3476-3514m)
This unit is lower most member of Pabdeh Formation that separates Pabdeh Formation from underlying Gurpi Formation. The member mainly consists of pale brown to pale red and medium grey to light grey marl with trace of thin bedded dusky green shale and light yellowish grey to off white limestone.

Gurpi Formation (3514-3915m)
Upper part of the formation comprises of very light grey, light grey, off white argillaceous, pyritic limestone with minor olive grey, medium grey to dark yellowish brown marl and trace of medium dark grey to dark green grey pyretic claystone with deep pelagic fauna of upper most cretaceous. The middle part of Formation comprises of light olive grey, olive grey to medium dark grey slight silty, locally pyretic marl interbedded with very light grey, yellowish grey to olive grey pyretic, argillaceous limestone with minor olive grey to dark green grey shale. Limestone with neritic fauna in middle part from paleontological point of view corresponds to the Lopha Member of Gurpi Formation. Lower part of the formation mainly consists of pale yellowish brown, light brown grey and light olive grey pyretic limestone with trace of glauconite in lower most part. Gurpi Formation formally divided into five members:

Emam Hassan member (3537-3569m)
It consists of off white, very light grey to light grey and minor dark yellowish brown to olive grey microcrystalline, argillaceous, chalky type limestone which is in partly pyretic with minor yellowish brown, olive grey to medium dark grey marl. It contains Maastrichtian foraminifers (Psedutextularia, Glt. stuarti and Glt. gansseri).

Dark grey shale and marl member (3569-3620m)
This unit separates the two carbonate units of the Emam Hassan and Lopha members. It mainly consists of dark yellowish brown, olive grey to medium dark grey marl alternating with very light grey, yellowish grey to off white argillaceous, pyretic limestone with trace of medium dark grey to dark green grey claystone.

Lopha member (3586-3763m)
It consists of light grey to medium light grey and minor olive grey to medium dark grey in partly pyretic limestone interbedded with olive grey to medium dark grey marl. The unit contains abundant shell fragment of Lopha Sp. and of benthic forams.

Grey marl and shale member (3763-3915m)
This unit consists of two parts in Azar-2. The upper part comprises of light olive grey to olive grey in partly pyretic marl with minor olive grey, brownish grey to dark green grey shale and rare light olive grey to medium grey limestone. Lower part of unit consists of pale yellowish brown to light brownish grey argillaceous, in partly pyretic limestone. At the contact with Ilam Formation, this limestone grading from yellowish grey to cream with neritic facies and glauconite.

2.2.2.3 Bangestan Group

Bangestan Group is divided into four formations Ilam, Surgah , Sarvak and Kazhdumi:

Ilam Formation (3915-4052m)
This Formation comprises of buff, yellowish grey, pale yellowish brown and light olive grey micritic, argillaceous, glaconitic and locally pyretic limestone interbedded with dark green grey, dark brown to dark grey marl and claystone in upper part. Buff, cream to very light grey clean, moderate hard limestone in lower part. Presence of micro pyrite as lamination/ nodule/pellet/aggregate in olive grey to pale grey limestone reported from 3920m to 3930m (about 5 to 10m below the top of Ilam Formation) could be consider as a key bed.
Ilam Formation contains both pelagic and neritic facies.

Pelagic Facies (3915-3991.5m)
It consists of buff, yellowish grey, pale yellowish brown and light olive grey micritic, argillaceous, glaconitic and locally pyretic limestone interbedded with dark green grey, dark brown to dark grey marl and claystone in lower part. The main fossil content of this sequence is pelagic forams.

Neritic Facies (3991.5-4052m)
This sequence mainly consist of clean, buff, cream to very light grey limestone with abundant neritic forams.

Surgha/Laffan Formation (4052-4059m)
This Formation consists of dark brown to black pyretic bituminous shale in type section and becomes highly argillaceous towards the base. It may contain a distinctive bed of limestone layer at middle part of the Formation, which is used as litho marker in the area. In Azar-2, the Formation comprises of buff, cream to light olive grey limestone in upper part and pale to dark yellowish brown limestone in lower part. There was no any indication of shale and marl in cutting samples in Azar-2.

Sarvak Formation (4059-4668m)
This formation is separated into 3 main units:

Upper Sarvak (4059-4373.5m) (Rumaila and Mishrif Equivalent)
It mostly consists of buff, cream to light yellowish grey microcrystalline, dense limestone in upper part of the section (Mishrif Equivalent). In the lower part of the sequence (Rumaila Equivalent), yellowish grey, light olive grey and brownish grey, argillaceous, chalky type limestone. In Upper Sarvak, about 55 meters below the formation top, two Gamma ray peaks observed on logs which are representative for presence of glauconite and pyrite in rocks. The distance between two peaks are 14 meters and lithology is Limestone. These peaks could be corresponds to two karsts surface in Upper Sarvak. See also Core # 1.

Middle Sarvak (4373.5-4400.5m) (Ahmadi Member Equivalent)
It is consists of dark grey, greyish black and dark brown, argillaceous limestone which locally contain micro pyrite and glauconite. The limestone is generally very argillaceous and locally grading to marls. Presence of abundant Oligostegina sp. (pelagic basinal foraminifers) is representative for this sequence.

Lower Sarvak (4400.5-4668m) (Maddud Equivalent)
This interval consists of very light grey, yellowish grey, light brownish grey to olive grey, microcrystalline, chalky type limestone. The limestone is generally clean to slightly argillaceous, locally slight dolomitic. At lower part of sequence, 118 meters of cherty limestone is observed. At the most lower part of section (35 meters above the contact with Khazdumi Formation), the limestone changes grading to olive grey, yellowish brown-dark yellowish brown, glauconitic, argillaceous, chalky type limestone.

Kazhdumi Formation (4668-4762m)
This formation formally consists of three distinctive parts in this area. In Azar-2, the lower contact of Kazhdumi Formation is not encountered and drilling stopped at 4762m where it seems the lower part of Kazhdumi Formation (Burgan) is just touched.

Upper part (4668-4702m)
It consists of olive grey, dark brown and medium dark green microcrystalline, argillaceous limestone which locally grading to marl. Upper most part of Kazhdumi Formation is identified by a significant increase in glauconite content in the limestone beds. A thick olive black-brownish black, bituminous Marl bed (5 meters thick) encountered 20 meters below the top of Kazhdumi Formation in Azar-2. This marl bed is about 14 meters above the first appearance of Orbitolina limestone and could be consider as a key bed in Kazhdumi Formation.

Middle part (4702-4759m) (Orbitolina Limestone)
It mainly consists of pale yellowish brown to olive grey, argillaceous limestone with trace of pyrite and glauconite particularly in upper part and trace of chert in middle part of the section. Abundant *Orbitolina sp.* is characteristic of the sequence and because of this the sequence could be age equivalent of Maddud member. First appearance of *Orbitolina Sp.* reported from 4709 meters, about 40 meters below Kazhdumi Formation top.

APPENDIX B – Core Data

6.5.2 Reservoir zonation and layer description

The following is a zone-by-zone overview of the Azar Sarvak reservoir zonation. The reservoir zonation for Azar-2 is tabulated in The reservoir zonation scheme (Figure 6-4, Figure 6-7 and Figure 6-8) is derived from the litho and sequence stratigraphic scheme established at outcrop in the Anaran Anticline, and is based on correlation of transgressive-regressive cycles and chronostratigraphically significant stratal surfaces where possible (i.e. maximum flooding surfaces, flooding surfaces, transgressive surfaces and sequence boundaries). The descriptions are mainly taken from the Azar-2 well. All depth references are in meter MD RKB (loggers depth), if not otherwise stated.

Azar-2					
Formation Name	Zonation name	Zonation No in RMS	Zonation top (m MD)	Zonation top (m TVD MSL)	Zonation thickness (m)
Upper Sarvak	USA	6	4059.00	3938.54	55.34
Upper Sarvak	NoNameShale	7	4114.35	3993.88	1.60
Upper Sarvak	USB	8	4115.95	3995.48	30.05
Upper Sarvak	USC2	9	4146.00	4025.52	104.99
Upper Sarvak	USC1	10	4251.00	4130.51	122.56
Upper Sarvak	USD	11	4373.56	4253.07	27.02
Lower Sarvak	LSA	12	4400.58	4280.09	22.22
Lower Sarvak	LSB	13	4422.79	4302.31	15.50
Lower Sarvak	LSC_D	14	4438.27	4317.80	27.70
Lower Sarvak	LSE	15	4466.11	4345.50	52.94
Lower Sarvak	LSF	16	4519.25	4398.44	52.88
Lower Sarvak	LSG	17	4572.30	4451.32	68.67
Lower Sarvak	LSH	18	4641.19	4519.99	27.50

Table 6-5: Azar-2 formation top zonation depths and thicknesses in RMS

Upper Sarvak A (USA)

Top USA is marked by an abrupt contact to claystones of the overlying Surgah Fm. Based on outcrop and cuttings data this contact is interpreted as a combined exposure and transgressive surface.

In Azar 2, reservoir unit USA is 55m thick and comprises a relatively homogenous package of ramp interior peloidal–miliolid wackestones to packstones capped by a probable exposure surface (karst). The matrix of the USA generally seems to be relatively tight. In intervals log porosities over 10% are evident (associated with rudistic and dolomitic facies). Visual estimates of porosity in thin section reveal values typically below 5%, with local peaks in the order of 10% (fractured dolomitic limestones and pure dolostones).

No Name Shale (NNS)

Top NNS is marked by an abrupt contact to dolomitic limestones of the overlying USA.

The No Name Shale forms a thin (circa 1.5m in Azar 2) calcareous mudstone break between units USA and USB. This interval comprises pelagic-outer ramp facies developed in association with Maximum Flooding Surface K140 (MFS K140 of Middle Turonian age). The No Name Shale forms a regionally correlatable marker throughout wells and outcrops in the Lurestan area. At

outcrop the No Name Shale is associated with elevated Total Organic Content's (TOC's). The unit also forms a permeability barrier/baffle and effective barrier to fractures (outcrop data).

Upper Sarvak B (USB)

Top USB is marked by an abrupt contact to calcareous mudstones of the overlying NNS. At outcrop and in core in Dehluran (e.g. Dehluran 3, 6) this contact is a major karst surface separating the Cenomanian Cycle 1 below from the Turonian Cycle 2 above. In Azar-2 a reddish silty cutting with quartz grains was seen at 4121m MD. This facies is comparable to karst fill seen at top USB in Anaran Anticline outcrops.

USB is a very heterogeneous interval, characterised from top to base by tightly cemented peloidal grainstone, porous and oil stained dolomitic-chalky rudist wackestones-packstones, porous oil-stained dolomite, tight phosphate-glauconite-spicule-dolomite wackestones-packstones and a basal low porosity interval of oligosteginid wackestones. This facies sequence appears to reflect shallowing upwards from outer to shallow ramp. The reservoir quality of USB is very heterogeneous, from tight to porosities of 10-15% in the better parts.

A circa 10m core (core 1) was cut between 4113.38-4123.32m core depths (Azar-2). Spectral core gamma and wireline logs run in the well indicate a shift of circa 9m between drillers depth (DD) and loggers/measured depth (MD). A distinct uranium spike at 4118.5m in the core spectral gamma can be correlated to a gamma spike at 4127.5m on the well wireline logs. The uranium is probably related to the abundance of phosphate at this level (interpreted MFS, widely seen in outcrop studies). The core appears to have been cut in a relatively dense zone (glauconite-phosphate dolomitic spiculite and karst zone) under the main interval of reservoir potential. Whole and plug measurements typically indicate porosities under 2% and permeabilities under 0.5 mD in the core.

Facies core description of core #1

Unit 1 - 4113.38 – 4114.38m. Finely crystalline lime mudstone (micrite) with a few silt to lower very fine sand sized particles. Possible packstone-grainstone fabric at base, with visible glauconite grains. Thin black mudstone partings at 4113.48 and 4113.82m. This interval is visibly etched by HCL (used to release the stuck core barrel), with common undulating wavy lamination, stylolites and stylocumulates weathering "proud" from the matrix. Differential compaction/pressure solution and/or bioturbation could be responsible for forming nodular bedding.

Unit 2 – 4114.38 - 4115m. Generally massive cemented featureless unit. Possibly a dolomitic pack-grainstone. Increasingly nodular bedded downwards. Questionable solution enlarged fractures at top of unit.

Unit 3 – 4115 - 4117.54 m. Nodular bedded wackestone to packstone with greenish-grey mudstones/argillaceous mudstones defining bedding breaks. Pervasive nodular texture related to bioturbation and stylolites. Numerous anastomosing stylolites with thick stylocumulates up to 3mm producing a nodular appearance to the core. Top and base unit 3 defined by a green (glauconitic?) wavy mudstone break giving a distinctively nodular bedded interval (looking almost conglomeratic). Short calcite-filled fractures evident between 4117-4117.38m, with bitumen fills locally. Fractures seem to cut across stylolites locally, but are more commonly cut by stylolites.

Unit 4 - 4117.54 - 4118.48m. Nodular bedded wackestone to packstone with anastomosing stylolites. Overall very tightly cemented. White bioclasts and dark grains (Phosphate?) up to 2mm across are seen scattered throughout unit. A phosphatised fish vertebrate is evident at 4118m. Nodules are separated by argillaceous/calcarenitic seams rich in phosphate and glauconite. Grains size is up to medium-coarse sand. The argillaceous lithology is filling *Thalassinoides sp.,* burrows. The basal 50cm of unit 4 is light white in colour and contains less stylolites. The texture appears to be packstone-grainstone.

Unit 5 – 4118.48 - 4119.66m. Light grey dolomitic packstone to wackestone cut by white dolomitic packstone-grainstone filled burrows or solution pipes. Typically white clay lining the edge of burrows (1-2mm thick) and central fill of white packstone-grainstone rich in glauconite and phosphatic debris. These lithologies are piped down from basal part of unit 4 above. Burrow intensity and abundance of glauconite-phosphate shows a gradual increase upwards. There is a candidate karstic surface / firmground at c. 4118.48 m. Here, large *Thalassinoides sp.,* burrows filled with white packstone-grainstone (?) penetrates dark, possibly reduction-stained lime mudstone. These *Thallassinoides sp.,* structures continue down to at least 4119.66 m, where they are filled with finely crystalline wackestone-packstone containing common glauconite.

Unit 6 – 4119.66 - 4123, 32m (Note, Interval from 4123-4123, 32m is stuck in barrel). Light grey to off white, very finely crystalline wackestone with irregular stylolites and anastomosing clay seams imparting a "nodular" appearance. Small 5mm-1cm across clay-lined burrows. Bioturbation index possibly very high, in part defining the nodular appearance. Green-clay breaks and glauconitic-phosphatic debris start to appear in upper part of interval, showing a transitional contact to unit 5. Short sub-vertical calcite-filled veins/fractures with possible solution enlarged edges. Fractures terminate abruptly at clay or stylolite seams.

Fractures core description: Generally, the core is not particularly fractured and the fractures identified appear to have negligible reservoir potential. Fractures are less frequent where stylolites and anastomosing dissolution seams are common. The main types of fractures are irregular, sub-vertical, sinuous, calcite-cemented fractures with 0.5-3 mm width and a few centimetres length. They are often truncated by stylolites or taper out. These fractures are more common in the lower part of the cored interval within the wackestone/mudstone facies containing glauconite-filled solution pipes and burrow fills. Closed fractures are more common in the upper mudstone facies with sparse stylolites. One fracture had a small insignificant aperture locally developed. Interestingly, several of the fractures appear to contain hydrocarbon inclusions.

Upper Sarvak C2 (USC2)

Top USC2 is picked at an oligiosteginid flooding event at the base of the overlying unit USB over mid ramp facies of upper USC2. The boundary is picked on a gamma high, and is also a clear facies change on FMI logs.

Unit USC2 can be further subdivided into three sub-zones, USC2-3, USC2-2 and USC2-1. Unit USC2-3 comprises mid-shallow ramp bioclastic algal-molluscan wackestones-packstones with visible oil-stained chalky microporosity and increasing gas readings towards the base of the zone. Log quality is poor in this interval due to poor hole conditions, precluding a full assessment of

reservoir quality. Cuttings indicate relatively poor reservoir with just patchily developed microporosity.

Taken collectively, zones USC2-2 and USC2-1 are associated with the most promising hydrocarbon shows, mud-cake build up, visible oil-stained micro/chalky, mouldic and local intercrystalline porosity in thin section, and elevated log porosities (3-13%). These two zones have the bulk of the log pay in Upper Sarvak, and represent a significant OIP volume. The matrix is relatively tight (1-5 mD based on RFT), and limited fractures are identified on the FMI log. Limited separation between the deep and shallow resistivity logs appears to confirm a low permeability matrix. Test 6 was completed in this interval. Thin section facies are dominated by relatively homogenous outer to mid ramp bioclastic wackestones, and wireline log and image log data indicate relatively common bedding parallel nodular chert and/or cemented limestone horizons. Calibration of cuttings to log data also indicates that elevated porosities are typically associated with fractured dolomitic wackestones with visible hydrocarbon staining. Porosity creation is thought to be related to a combination of early meteoric dissolution, followed by porosity enhancement by hydrothermal leaching resulting in chalky microporosity and subordinate dolomite development along the same intervals affected by early meteoric dissolution.

Upper Sarvak C1 (USC1)
Top USC1 is marked by an abrupt change from low gamma values at the top of USC1 to higher values in the overlying USC2. Image log data also show a facies change at this point, as do cuttings data (marked shallowing from top of USC1 to base of USC2).

Unit USC1 can be further subdivided into three sub-zones, USC1-3, USC1-2 and USC1-1. These units are dominated by outer ramp and pelagic oligosteginid-calcisphere wackestones to mudstones, including calcareous turbidites. Chalky microporosity and micro-fractures are evident in cuttings, typically associated with scattered dolomite development. Matrix porosities are low (3-8%), and the success of Test 5 in the USC1-3 interval could be attributable to open fractures visible on FMS data and evidenced by dynamic mud losses. Test 5 can be correlated with the top of zone USC1-3 (Top Rumalia) in the Badra-1, Changuleh-2 and Dehluran wells. In Changuleh-2 porosity in this interval is generally under 3%.

Rate Of Penetration (ROP), cuttings, resistivity, neutron porosity, gas readings and shows all indicate that the interval between 4250-4268m is the main log pay zone in USC1-3.
A dramatic increase in resistivity below 4294m MD associated with the presence of asphalt in cuttings appears to indicate a zone of dead oil in units USC1-2 and USC1-1.

Upper Sarvak D (USD)
Top USD is marked by an abrupt change to lower gamma calcareous turbidites of overlying USC1. USD forms the basal unit of the Upper Sarvak Fm, and in Azar-2 comprises a 27m interval of pelagic-outer ramp mudstones and micritic carbonates. USD is equivalent to the Ahmadi Member, which represents a regionally correlatable MFS of earliest Cenomanian age (K120 of Sharland et al., 2001). The Ahmadi Member separates the Lower Sarvak Fm below from the Upper Sarvak Fm above. At outcrop in Lurestan the Ahmadi Member is associated with elevated TOC's, and is a possible source interval for overlying reservoir units. In Azar 2 matrix porosities are typically under 3%, but open fractures with oil are seen in cuttings. USD could form an effective barrier between

the Lower and Upper Sarvak in the absence of significant fracturing. USD is of relatively uniform thickness development in the Anaran exploration block.

Lower Sarvak A (LSA)

Top LSA is marked by an abrupt flooding event (Transgressive Surface) to overlying hemipelagic facies of USD (Ahmadi Member, Upper Sarvak Formation). Top LSA might also be associated with subaerial exposure (outcrop thin section data) and "leaching" to account for the chalky porosity evident within top LSA in the Azar-2 well.

In Azar-2 unit LSA comprises a 22m thick interval of shelf interior to margin wackestones interbedded with pack to grainstones. Unit LSA appears to comprise a simple shallowing upwards cycle based on well log and cuttings data, with a "fining up" top related to the passage to muddy

shelf interior facies, that are in turn abruptly overlain by deeper water facies of the Ahmadi Member. Porosity development is most pronounced in the upper 5m of LSA within "muddier" facies (up to 10% Ø). Cuttings thin section observations indicate that this porosity is most likely chalky microporosity and mouldic-intraparticle porosity, possibly related to leaching at the Top Lower Sarvak surface. Image log data show what appears to be well-developed vuggy porosity. A similar porosity development is thought likely in Badra-1 and Changuleh-2 based on wireline log data.

The basal part of LSA-top LSB is also associated with a porous interval with good gas and HC shows. Image log data indicate patchy porosity development, interpreted as vuggy, patchy bioturbation and/or rudist related.

Lower Sarvak B (LSB)
Top LSB is picked at a distinctive higher gamma interval. At outcrop this higher gamma event is associated with a flooding event, with in-situ rudist shoals overlain by thin *Exogyra sp*., bearing dark micrites. This gamma spike can be correlated at the base of LSA in the Badra-Azar-Changuleh-Dehluran wells, and is interpreted as a regionally developed flooding event. On the spectral gamma log in Azar-2 it is clear that this event is associated with a uranium spike within a carbonate lithology.

In Azar-2 LSB forms a 15m thick interval of generally non-poor matrix reservoir interval of muddy carbonates interpreted to have been deposited in lagoonal/shelf interior to shelf margin (base LSB) to outer shelf (top LSB) environments. These two facies types are separated by a flooding event (based on cuttings thin sections, correlation to outcrop sections and wireline logs) picked at circa 4427m MD in Azar-2. This flooding event can be correlated with relative ease between Badra-1, Changuleh-2, Dehluran and outcrop sections. Log signature in LSB in all wells is comparable, showing increasing gamma upwards, interpreted to reflect increasingly muddier/fine grained carbonates upwards.

Lower Sarvak C_D (LSC_D)
Top LSC_D is marked by a change from the low gamma values of unit LSC_D to increasingly higher gamma values in the overlying unit LSB. This contact coincides with a change from *Orbitolina sp*., dominated facies below to rudist-algae dominated facies above and represents a gradational back stepping contact to more shelf interior facies within USB.

LSC_D is 28m thick in Azar 2, and form two distinctly correlatable units based on gamma log, cuttings and outcrop data, but from a reservoir facies perspective they can essentially be treated as one unit. LSC_D is dominated by *Orbitolina sp*., packstones-grainstones interpreted to have been deposited as a high-energy carbonate shoal/sand complex developed in a mid ramp/platform to shelf/ramp margin location. The flooding event at the base of LSD is overlain by one main shallowing and "coarsening" upwards progradational cycle from muddy toesets at the base to cross bedded *Orbitolina sp*., packstones in the foresets to topsets. This is reflected on the gamma log response (cleaning upwards signature). Individual set boundaries/cross beds are cemented, giving the characteristic erratic resistivity response in this unit. The cemented nature of these sets is confirmed by Core 2 (Azar-2), image log and outcrop data. This results in a reduction in net pay. Correlation between Badra-1 and Changuleh-2 indicates better reservoir quality in Badra-1 and decreased reservoir quality in Changuleh-2. This is interpreted to reflect a higher energy shelf

margin location in Badra-1 and a more protected shelf interior setting in Changuleh-2. Cementation of set boundaries also appears to be limited in Badra-1.

Log porosities in LSC_D are typically between 9-15% excluding the cemented horizons and the basal mudstone, which may form a low Ø/Kh baffle. Low matrix permeabilities are reflected by limited separation in the deep and shallow resistivity logs and limited mud cake build up. Whole core porosities and permeabilities give values of 13-15% (porosity) and 1-17mD (permeability). Cuttings data and the PEFZ data indicate a relatively clean limestone with limited dolomite development. Pore types include inter and intra particle, vug, chalky and mouldic porosity with localised fracture porosity. Hydrocarbon is not commonly observed in thin section, but significant shows and gas readings were recorded at wellsite and the cuttings thin sections indicate that a range of different pore types are present through this interval that appear to combine to provide an effective reservoir as indicated by Test 4.

Core 2 (3m recovery) was cut in the upper part of LSD, and generally confirms the above facies descriptions. Core porosities are typically in the order 13-15%. Whole core permeabilities vary from 1.1 to 17mD. In addition, the core is cut by numerous bedding parallel open fractures with visible oil stain. The fractures follow cementation fronts and stylolites. Vuggy porosity is locally developed (vug size typically up to 5mm). Porosity distribution is very heterogeneous, and clearly secondary enlarged associated with the development of chalky microporosity, vuggy and enlarged interparticle porosity.

Results of whole core analysis:
5 samples were selected for whole core analysis (Table 6-). Selection was based on intervals with minimal fracturing so as to obtain matrix permeabilities. Nevertheless, the relatively homogenous porosities, but varied permeabilities are thought to reflect the role of fractures.

Table 6-6: Core analysis Azar-2 core #2

Company : Hydro Zagros Oil & Gas — File No. : 50332 .
Well : AZAR . 2 — Date : 8-Aug-2005
Country : Islamic Republic of Iran — Analyst : AM/MH

Preliminary Data

WHOLE CORE ANALYSIS

Sample No.	Depth (m) From	Depth (m) To	@ Ambient Conditions Ø(He) %	Kair (Max) md	Kair (90°) md	Kair (V) md	Grain Density gm/cc	Description
CORE NO. 2 DEPTH INTERVAL (4432.00 to 4434.96 m)								
4	4432.40	4432.60	14.9	5.8	5.5	1.1	2.71	chipprd
5	4432.68	4432.82	13.7	4.0	2.7	0.37	2.71	frac along Hz direction
6	4432.84	4432.97	14.2	1.1	0.66	0.51	2.72	
7	4433.00	4433.10	12.9	17.	9.7	5.8	2.72	closed frac
8	4434.08	4434.17	13.3	13.	6.5	0.63	2.71	frac along Hz direction

6.6 Matrix property model

The matrix porosity is modelled using the "Petrophysical modelling" module of RMS. The matrix permeability and water saturation has been derived from the porosity parameter. The Ilam and Upper Sarvak data from the Changuleh West-1 well is included in the model. Since no log data were available for the Lower Sarvak Formation in Changuleh West-1 (fish in hole), Changuleh West-1 has not impacted the Lower Sarvak part of the model. Overall the Changuleh West-1 result came in as predicted by the preliminary MDP model (i.e. pre Changuleh West-1), apart from somewhat poorer properties in the USC2.

6.6.2 Matrix porosity

The matrix porosity is modelled by running stochastic simulations in RMS with 3D trends as an important part of the transformation sequence. The 3D trend is utilised to be able to implement the lateral large-scale trend of improved porosity when going from SE (Changuleh-2) towards NW (Badra-1). This trend is motivated by the well data and supported by the Paleogeographic maps. Increased dolomitization due to a more distal position (closer to the magnesium rich paleo sea) may explain the increase of dolomitized limestone and dolostone seen in Badra-1 (cuttings) and hence the picture of increased porosity towards NW (see chapter 6.4 for a description of the conceptual geological model and reservoir development). Note that the 3D trend only has lateral variations. The z direction has constant values for each sub-grid. The 3D trend parameter is constructed by

using the "Parameter trend modelling" functionality in RMS with lateral trend surfaces as input. The lateral trend surfaces are gridded in RMS using the zonal well averages (for each sub grid) as input (see Figure 6-20 for example of matrix PHIE trend map). For most of the sub grids the porosity shows a logarithmic distribution. Therefore logarithmic transformations are applied before applying the logarithm of the 3D trend. After this a vertical depositional trend transformation is applied before a final mean adjustment is performed as the last part of the transformation sequence.

The result of the methodology described above is a model that honours the large-scale lateral trend of improved properties towards the NW, but at the same time by utilizing the stochastic petrophysical simulation technique incorporates the small-scale variability/heterogeneity of the porosity distribution (Figure 6-21, Figure 6-22 and Figure 6-23 illustrate the modelled/simulated matrix porosity (before cut-off)). The average simulated porosity is somewhat lower than the blocked well porosity, 2.8 vs. 3.1%, respectively, see Figure 6-24. See next section in this chapter for a further description. The modelled/simulated porosity is perfectly conditioned to all the input blocked well data (Figure 6-25). An illustration showing the blocked well porosity of Azar-2 together with an x-section view of the modelled porosity parameter (before applying cut-off) is shown in Figure 6-26.

After the porosity modelling a 4% cut-off is applied on the porosity by setting all values in the porosity parameter below 4% to 0% porosity (see chapter 7.4.4 and chapter **7.10** for further discussion of cut-off). In chapter 6.9.4 a sensitivity study on the effect of cut-off on matrix STOOIP is presented. Figure 6-27, Figure 6-28 and Figure 6-29 illustrate an example map and x-sections through the PHIE_4 parameter (porosity parameter with 4% cut-off applied). Isoporosity maps can be found in Appendix 6: Matrix Isoporosity Maps.

6.6.3 Matrix permeability

The matrix permeability is calculated using equations from NH Carbonate atlas (Ref Lønøy, A., 2006. Making Sense of Carbonate Pore Systems. American Association of Petroleum Geologist, pp. 1381 - 1405) with one equation for each sub grid. The dominant pore type for each sub grid is identified from cuttings (Azar-2) and defines the type of equation chosen from the Atlas (see Figure 6-33 for example of equation). The equation is giving a direct relationship between matrix porosity (input) and matrix permeability (output) and is implemented in the RMS model as an IPL script. With this technique the modelled matrix permeability will have the same general large-scale trend as the matrix porosity. The input matrix porosity to the equations is the modelled/simulated porosity parameter after applying 4% cut-off (PHIE_4 parameter of RMS model).

Correlations between matrix permeability (Kh_PHIE4) and matrix porosity (PHIE_4) for Azar:

Sub grid=6 and 7 Kh_PHIE4=(Exp (PHIE_4*44.47))*0.0036
Sub grid=8 Kh_PHIE4=(Exp (PHIE_4*43.99))*0.0037
Sub grid=9, 10 and 11 Kh_PHIE4=(Exp (PHIE_4*42.72))*0.0037
Sub grid=12 Kh_PHIE4=(Exp (PHIE_4*69.91))*0.0028
Sub grid=13 Kh_PHIE4=(Exp (PHIE_4*43.91))*0.0037
Sub grid=14 Kh_PHIE4=(Exp (PHIE_4*43.15))*0.0045

Sub grid=15 Kh_PHIE4=(Exp (PHIE_4*44.05))*0.0039
Sub grid=16 Kh_PHIE4=(Exp (PHIE_4*41.01))*0.0049
Sub grid=17 Kh_PHIE4=(Exp (PHIE_4*42.61))*0.0039
Sub grid=18 Kh_PHIE4=(Exp (PHIE_4*43.24))*0.004

A sensitivity study shows that the interpreted pore type is not critical for the calculated permeability. The main reason is that the poro-perm equations are converging when the porosity is low, as for large parts of Azar.

Figure 6-34 illustrates the modelled matrix permeability (Kh_PHIE4 parameter in RMS model). The permeability shows a logarithmic distribution with a mean of 0.19 mD. Figure 6-35, Figure 6-36 and Figure 6-37 illustrate maps and x-sections through the modelled/simulated permeability parameter (Kh_PHIE4 of the RMS project).

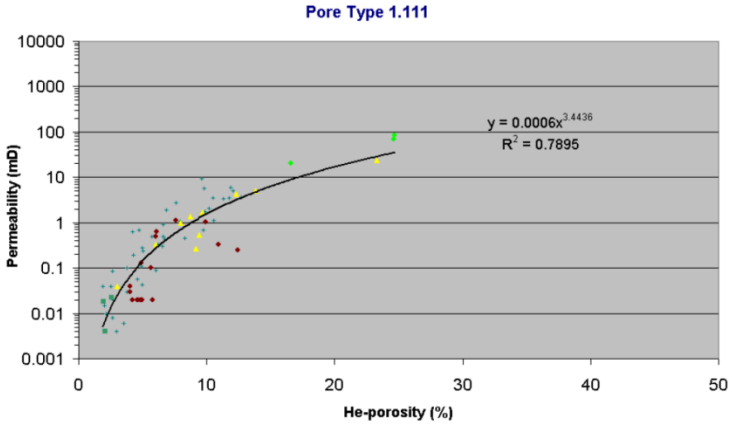

Figure 6-33: Example of poro-perm relationship for one of the dominant poretypes of Azar - Interparticle Microporosity, Patchy distribution (pore type 1.111). Norsk Hydro's carbonate atlas

6.6.4 Matrix water saturation (Sw)

The matrix water saturation (Sw) is calculated based on correlations of Ø, Kh and SWE. Porosity (Ø) is log-computed porosity, permeability (Kh) is computed from porosity and pore types and water saturation (SWE) is computed from logs with Archie's equation.

SWE correlations with Ø, Kh, J, and $(Kh/Ø)^{0.5}$ were investigated, best SWE correlations were found between porosity and $(Kh/Ø)^{0.5}$ (equations for each sub-grid shown below). It was not possible to create a consistent model, i.e. a model that is matching all the well data. The Badra-1 well seems more consistent, with a potential J-function like behaviour. The Azar-2, Changuleh West-1 and Changuleh-2 seem to have less correlation to a J-function. This may be a function of the

better reservoir quality of the Badra-1 well together with a potential proximity to the oil-water contact. Further the Azar-2 well contain high water saturation above the fluid contact due to the presence of chalky micro-porosity, that prevents the proper correlation between log computed Sw and Sw estimated from capillary data. See chapter 7.8 for further description of the RMS matrix water saturation model.

A correlation between log SWE and log porosity or $(K/Ø)^{0.5}$ was implemented on the different zones (IPL script in RMS project):

Zones 1 to 9	Sw_PHIE4=Exp((-Log(Sqr_PHIE4)*0.857-0.271)*2.3026)
Zones 10, and 11	Sw_PHIE4=-Log(PHIE_4+0.0001)*0.509-0.489
Zones 12, and 13	Sw_PHIE4=-Log(PHIE_4+0.0001)*0.447-0.153
Zone 14	Sw_PHIE4=-Log(PHIE_4+0.0001)*0.960-0.531
Zones 15, 16, 17, and 18	Sw_PHIE4=-Log(PHIE_4+0.0001)*0.471-0.1765

In the equations above Sw_PHIE4 is the calculated water saturation parameter based on the porosity parameter with 4% porosity cut-off applied, PHIE_4 is the porosity parameter with 4% cut-off applied and Sqr_PHIE4 is the square root of (Kh_PHIE4 / PHIE_4). Kh_PHIE4 is the calculated permeability based on PHIE_4 (chapter 6.6.3).

The following cut-off's are applied on the modelled Sw parameter:

- Minimum Sw is set to 0.2 (= 20 %) to account for the irreducible Sw.
- Modelled Sw higher than 0.75 is set to 1 to account for the uncertainties in estimating Sw in areas of high water saturation.
- For porosities < 0.02 (= 2%) the Sw is set to 1 to account for oil not being able to migrate into the tight matrix of the chalky Microporosity. From a practical point of view this part of the IPL script will not affect the resulting Sw parameter, since all porosity < 4% has already been set to 0.

The modelled Sw parameter is not matched to the wells, but when comparing the model vs. well data for the Sarvak reservoir, inside the volume calculation polygon (Figure 6-79) and for values above the porosity cut-off of 4%, a good match is observed (Figure 6-40).

Map and X-sections of the final modelled Sw parameter (Sw_PHIE4 of the RMS project) are displayed in Figure 6-41, Figure 6-42 and Figure 6-43. Figure 6-38 and Figure 6-39 show the statistical distribution of the modelled Sw parameter (Sw_PHIE4). The water saturation is heavily skewed towards the upper values (i.e. Sw close to 1), reflecting the skewness towards low values for porosity and permeability.

For the fracture volume (see chapter 6.7 for fracture modelling) the Sw is assumed to be 0, i.e. the fractures are completely oil filled.